UNIVERSITAT POLITÈCNICA DE VALÈNCIA

motores térmicos

TRABAJO DE FIN DE MÁSTER

DEVELOPMENT AND VALIDATION OF A TWO-PHASE COMPUTATIONAL MODEL FOR AN ALTERNATIVE FIRE SUPPRESSION AGENT

Realizado por: Nishit Shaparia
Dirigido por: Antonio Gil Megías

Valencia, Noviembre de 2020

Máster Universitario en
Motores de Combustión Interna Alternativos,
Curso 2019-2020

INSTITUTO UNIVERSITARIO CMT-MOTORES TÉRMICOS

Abstract

Halon1301 has been used as a fire suppression agent in active fire extinction systems in aircraft engines, APU (Auxiliary Power Unit) and cargo fire protection for more than 50 years. In 1987, a research carried out by the Montreal Protocol shows that Halon is damaging the environment because of its ozone-depleting properties. Therefore, the use of Halon gases has been banned in the industry by the Montreal (1994) and Kyoto (1998) protocol. So, it is indeed to find replacement of halon gases which is more eco – friendly. Among these alternatives, Novec-1230 is a sustainable alternative that works quickly, cleanly and efficiently. The fire suppression system requires a specific concentration of the fire suppression agent (4-6 % for Novec-1230 and 5% for Halon) to be diluted in the air to extinguish the fire. The problem of changing the phase of the rapidly depressurized mist of a fire suppression system is a topic of high interest due to the effect of the modelling of these phenomena in a successful simulation to design these modifications. Due to the high difference of pressures between the container and the ambient, the discharge through the nozzle is expected to be critical. In this report, two different alternative fire suppression agents and two nozzles are used - Water and Novec1230.

The main goal of this project is to develop a new model for a two-phase Eulerian-Eulerian CFD U-RANS that can be used to reduce the computational cost and increase the accuracy of traditional approaches based on Eulerian-Lagrangian. These two approaches are performed with CFD commercial software (ANSYS–Fluent). As validation, spray performances such as spray penetration, spray cone angle are compared with experimental results.

UNIVERSITAT POLITÈCNICA DE VALÈNCIA

motores térmicos

Contents

CHAPTER 1

1 Introduction

1.1 Background and introduction

Nowadays, halon gases are used as fire suppression agents in most active fire extinction systems, due to its effectiveness and low toxicity. In 1987 A research carried out by Montreal Protocol shows that Halon is damaging the environment because of its Ozone Depleting properties. So, it is indeed to find replacement of halon gases which is more eco – friendly. Among other alternative agents, Novec1230 offers a number of important advantages over other clean fire suppression agents The main difference between Halon and Novec-1230 is their physical properties [Table 1], in addition to the lower global warming potential of the latest, its higher molecular weight. As a result, the boiling point at ambient pressure of the latter is much higher which results in a more difficult vaporization and dispersion.

The way a fire suppression system works can be summarized as follows: the fire suppression fluid is stored in a pressurized container. Another gas, such as Nitrogen, can be used to increase the pressure of the container. When the fire starts, the container is rapidly depressurized, and the fire suppression fluid is discharged through a nozzle.

Extinguishing agent	Halon1301	Novec1230
Chemical formula	CF_3Br	$C_6F_{12}O$
Chemical name	Bromotrifluoromethane	Pentafluoroethyl ketone
Ambient phase	Vapour	Liquid
Boiling point	-57.8 °C	+49.2 °C
Liquid density at ambient	1575 kg/m^3	1600 kg/m^3
Vapour pressure	2.5 bar	0.404 bar
Ozone depletion potential	5.1	0
Global warming potential	1300	1

Table 1 Key properties of Novec1230 and Halon1301

1.2 Description of the physical problem

A boarded halon fire extinguisher system may consist of only a bottle and a nozzle or a complex arrangement of pipes and nozzles [1]. Several multi-hole nozzles are typically used in systems designed for cargo cabin. To simplify the test rig and the following Computational Fluid Dynamics (CFD) validation, a nozzle with a single orifice oriented in the axial direction has been used in an experimental facility.

The analysis is divided into two zones: Study the process inside the nozzle or atomizer, and on the other hand, analyze the discharge outside the atomizer, Inside the nozzle, assumption made that the fire extinction agent (water or Novec 1230) is in the liquid state; i.e. the pressure inside the atomizer is considered higher than the ambient pressure, which is, in fact, higher than the saturation pressure for the temperatures of operation 268 K < T_{cargo} < 298 K (normal operating condition, T_{cargo} = 15 ºC, cold soak T_{cargo} = −5 ºC and hot discharge T_{cargo} = 25 ºC).

This liquid jet is inherently unstable and breaks up into droplets following one or several of the following break up regimes: Rayleigh regime, primary and secondary aerodynamic breakup regimes and, finally full atomization regime. The size of the droplets is of the same order as the nozzle diameter in the Rayleigh and primary breakup regimes, while it is much lower than the jet diameter in the secondary break-up and atomization regimes. For a thorough review of the jet break up phenomenology see below section. The atomization process is very complex and usually experimental correlations for the final distribution of sizes of the droplets are used [2].

1.3 Methodology

The main outline of this project is to develop CFD model to simulate the penetration of a two-phase flow and to model the phase transitions. The developed procedure should be valid to perform a parametric study relevant for the aircraft fire suppression system, using both the Eulerian-Eulerian and Eulerian-Lagrangian CFD U-RANS models. Therefore, this work presents an Eulerian model, which is the best approach to study dense mixtures. That model is capable of simulating the internal nozzle flow and the liquid vein atomization in the same domain (at the same time). Phase changes process such cavitation or evaporation are not considered. Second simplification is assumed mainly to reduce the complexity of the computational model as much as possible. From another point of view, it is well known that the nozzle geometric parameters have a great influence on the spray behavior, therefore, internal studies of nozzle is also carried out [41, 42]. from the internal flow simulation, some properties like velocity, mass flow rate, angle were captured as an input boundary condition for external flow. Thus, to couple the internal and external flow simulations of the spray atomization process leads to a better representation of reality and better understanding of the physics involved.

Spray modelling was achieved using DPM which account for an Euler-Lagrange approach. In DPM, continuous phase is solved using time-averaged Navier-Stokes equations. Unsteady particle tracking has been used to track the droplets. The commercial CFD package ANSYS Fluent was used for the simulations. All the simulations were performed using the pressure-based solver available in ANSYS Fluent [20].

Figure 1 shows the workflow methodology followed for developing the model. First, in the introduction, the physical problem is described and then, the two–phase flow models, including phase change, available in the literature are reviewed. Second, two different two–phase models (Euler–Euler VOF and Euler–Lagrange) are explained in detail. Later, Eulerian-Eulerian model was generated for both Nozzle 1 and 2 also, Eulerian-Lagragian model was developed for Nozzle 2. At last, the results available from CMT experimental facilities were compared to validate the model.

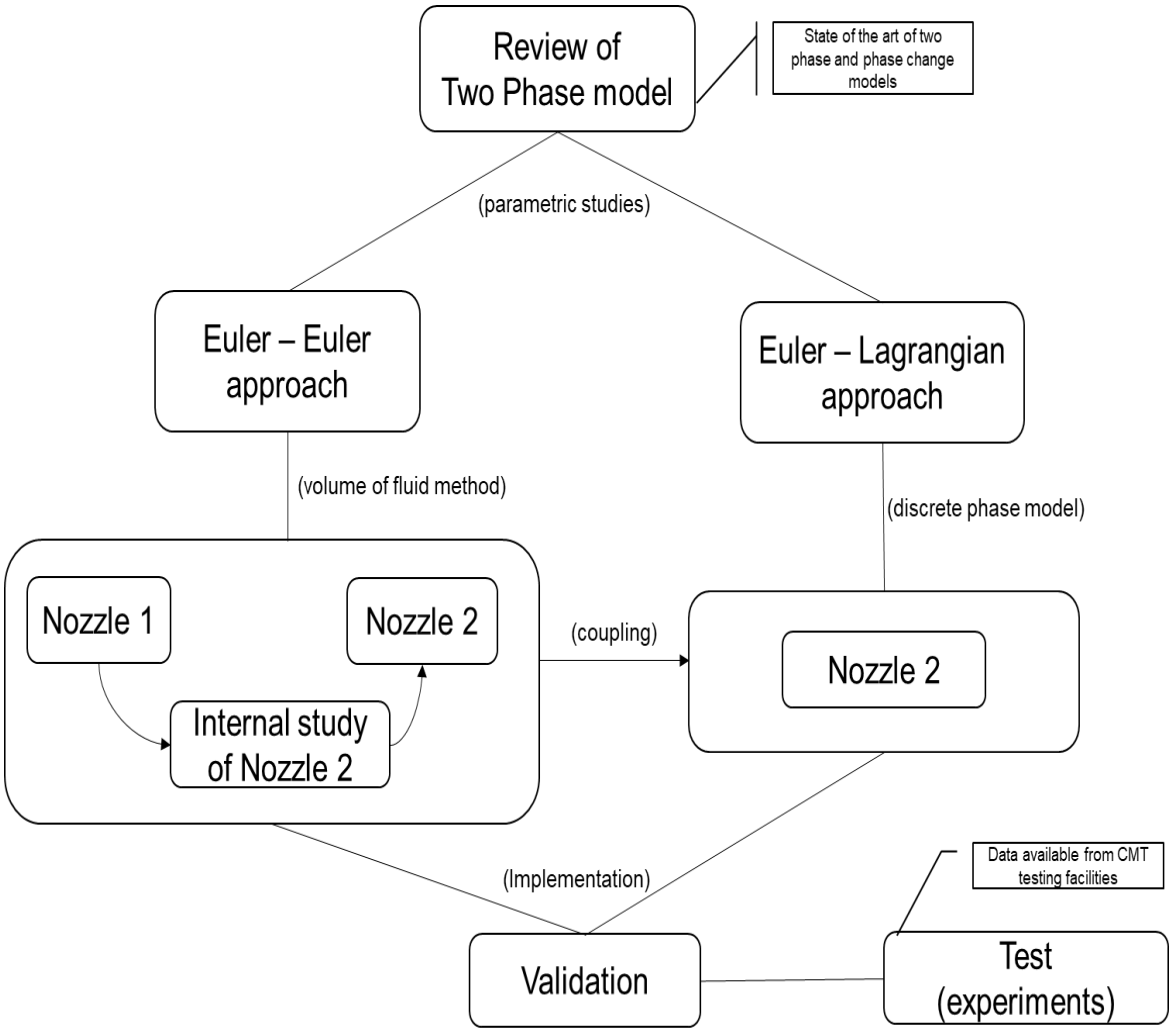

Figure 1 Workflow Methodology structure

CHAPTER 2

2 Fundamentals of Liquid Sprays

2.1 Atomization

Atomization is the mechanism that leads to an increase in the liquid-gas interfacial area inside a given control volume. It leads to pulverization of the liquid jet into multiple droplets which become smaller and smaller under the influence of atomization mechanisms. The break-up of the liquid jet is a consequence of interaction occurring at the microscopic scale, involving aerodynamic interactions and surface tension forces, ones promoting the liquid disintegration and others keeping it compact, respectively. As a result, it is caused by a sum of several independent effects, which depending on the injection conditions and the nozzle geometry, present different levels of influence [3–8]. According to the role of the turbulent flow and the aerodynamic forces on the spray break-up, the atomization process can be split into three distinctive zones: primary atomization, secondary atomization, and dispersed spray as shown in figure 2.

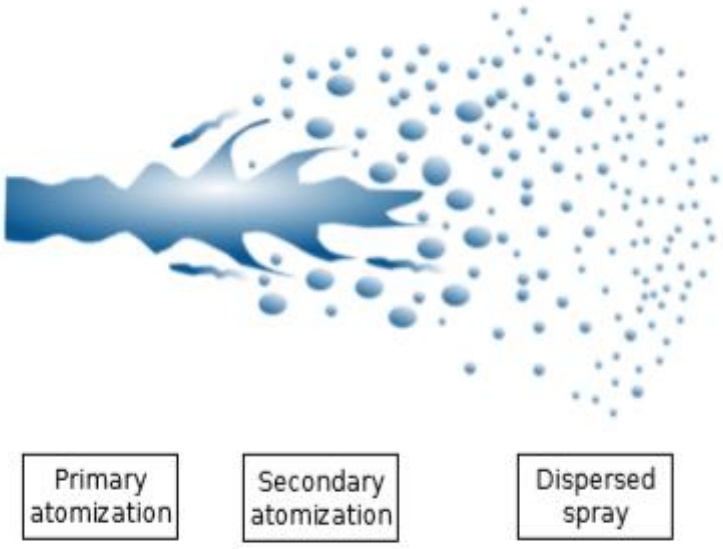

Figure 2 Distinctive zones in the atomization process

2.2 Primary atomization

The primary atomization process occurs once the liquid has left the injector nozzle. In this region, the high-velocity gradients between the liquid and the gas lead to shearing instabilities. These instabilities show sinusoidal waves at the liquid-gas interface in the direction of the liquid flow. The amplitude of waves will increase until provoking detachments of liquid structures from the liquid core. These structures remain relatively big compared to the liquid core size. This region where instabilities and first liquid detachments appear is called the primary atomization zone, also a dense zone of the spray. This break-up occurs due to the action of internal forces such as inertial instabilities, effects of the turbulent flow, the reorganization of the velocity profile at the nozzle orifice outlet [3] and the cavitation phenomenon.

2.3 Primary atomization regimes

Physical processes occurring during the atomization have been studying, both experimentally and theoretically, for many years. Starting with the Rayleigh [9, 10] theory for non-viscous fluids injected with low velocity, conditions at which atomization occurs due to surface tension forces. Then, the experimental studies conducted by Haenlein [11] motivate the theoretical parallel research by Weber [12], in which Rayleigh's theory was extended to viscous fluids and accounts for the effect of aerodynamic interactions. Following Ohnesorge [13] studies, where the transition between the different documented atomization regimes was investigated. Finally, the studies by Reitz [14,15], where the break-up regimes can be classified as follows for a cylindrical jet (see figure 3).

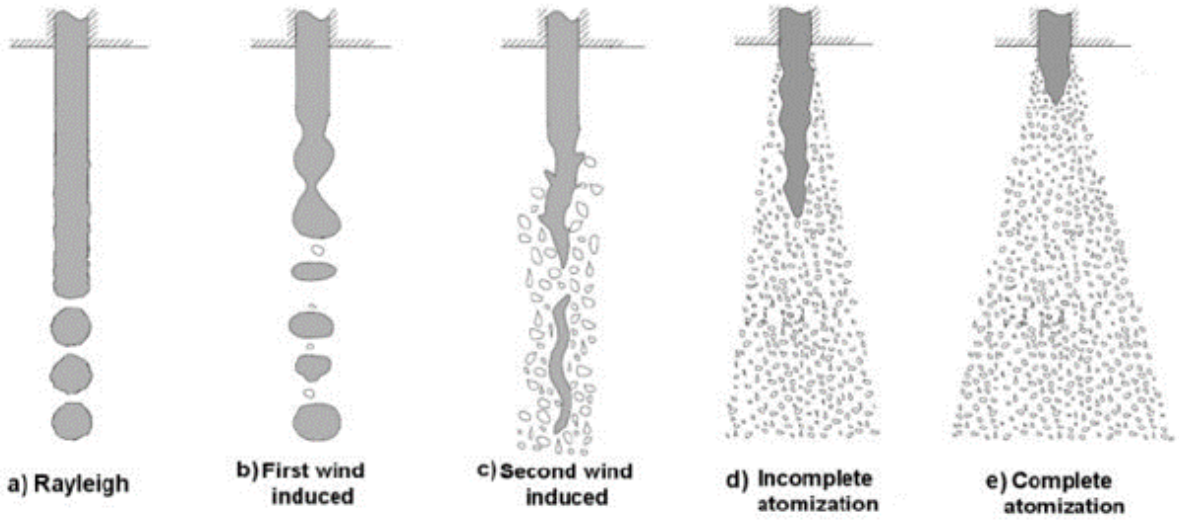

Figure 3 Break-up regimes

- **Rayleigh regime:** This regime is observed at the lowest jet velocities. In this case, the perturbations at the surface of the jet caused by the effect of surface tension deform the liquid vein until it is separated in droplets, whose sizes are uniform and larger than the outlet orifice diameter.

- **First wind-induced regime**: As a consequence of increasing velocity, the effect of the forces generated by the relative velocity between the jet and the surrounding ambient becomes more important. In this way, the friction forces effect plays the same role as the surface tension and ease droplet formation. In this regime, as in the first one, the droplets are generated far downstream of the discharge orifice and their size is similar to the outlet orifice diameter.

- **Second wind-induced regime:** Increasing again the jet velocity, the atomization process is more efficient. The initial perturbations are amplified by the aerodynamic forces and the break-up occurs closer to the orifice. The average size of the formed droplets is much smaller than the outlet orifice diameter (comparable to t$\partial\partial t$he wavelength of the initial perturbations).

- **Atomization regime:** The jet disintegration occurs in the immediate proximity of the orifice (closer as highest injection velocity). In this case, two possibilities are depending on the presence of the intact liquid core. Thus, two atomization regimes are commonly defined: incomplete and complete, in which the intact core can be observed or not. The size of the formed droplets is again much smaller than the outlet orifice diameter.

2.4 Dimensional analysis of the atomization process

The study of sprays is usually catalogued using the dimensionless numbers:

$$Re = \frac{\rho_l \, u \, D_0}{\mu_l} \qquad Oh = \frac{\mu_l}{\sqrt{\rho_l \, \sigma \, D_0}} \qquad We_g = \frac{\rho_g \, u^2 \, D_0}{\sigma}$$

where Re is the Reynolds number, We_g is the Weber number, Oh is the Ohnesorge number, u is the flow characteristic velocity, D_o is the characteristic length of the problem in this case it represents diameter of nozzle exit, ρ_l, μ_l are the density and the kinematic viscosity and σ is the surface tension between the gas phase and the liquid phase. These numbers may refer to both the liquid phase and the gas phase (e.g. in case of air assisted atomizer), hence the parameter choice is crucial for characterizing the problem. The nature of this number is well known in literature and is at the basic of flow description both from the macroscopic scale (e.g. when referred to the flow bulk) and for the microscopic scale (e.g. when referring to smaller scales of motion [16]).In general, in absence of gas flows that promote instabilities, the

atomization regime can be characterized by two of these dimensionless numbers and their density ratio[17], although this approach has a limited range of applicability and relies on the development of turbulence in the nozzle(even if not fully developed).

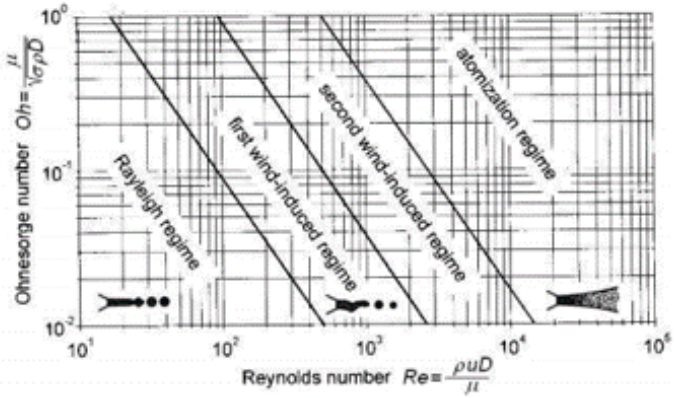

Figure 4 Ohnesorge diagram

In figure 4, the borders between the four atomization regimes are identified as in [18]. However, only the liquid properties are considered in this diagram, which results in insufficient because of not taking into account the ambient gas-phase effects (pressure-density), as evaluated by Torda [19].

2.5 Secondary atomization

Secondary atomization follows the primary atomization. Ligaments or relatively large droplets formed during the primary atomization are still moving at high speed in the discharged gaseous atmosphere and thus, aerodynamic forces affect them and cause a new disintegration which results in smaller droplets.

Further from the injector, liquid structures do not interact with each other anymore (or very weakly). At this scale, surface tension prevails. It minimizes the droplet surface and energy, leading to spherical droplets. This zone is called a diluted or dispersed spray region.

Droplets formed by the liquid jet break-up (primary atomization) are still moving at high speed in a gaseous atmosphere. The fate of the droplets is also decided by the same balance of forces already described, causing the so-called secondary break-up. Due to the difference in shape (spherical droplet instead of the cylindrical jet), the modality in which this process occurs is different.

Aerodynamic forces due to the relative velocity between the droplets and the gas tend to break them into smaller droplets. On the opposite side, forces associated with the surface tension tend to maintain the original spherical shape of the droplet. Therefore, it is harder, in other words, requires higher relative velocity to break smaller droplets because their curvature and so their surface tension is higher.

Two typical interactions in secondary atomization are coalescence and collision. In the coalescence case, two liquid structures encounter each other and unified to form a single entity. In the collision case, the two structures have different velocities and encounter each other in a more violent way that provokes their breakup and the creation of smaller structures [10, 11].

Further from the injector, liquid structures do not interact with each other anymore (or very weakly). At this scale, surface tension prevails. It minimizes the droplet surface and energy, leading to spherical droplets. This zone is called a diluted or dispersed spray region.

Chapter 3

3 Mathematical description of the problem

3.1 Two-phase flow regimes

Multiphase flow is not a canonical problem, therefore different models can be found in the literature. Two different approximations will be considered here: Euler-Euler (EE) models and Euler-Lagrange (EL) models. In EE models the two phases are treated mathematically as interpenetrating continua. On the contrary, in EL models one of the phases is treated as continua while the other as a dispersed phase. The selection of one or another model strongly depends on the problem to solve. The volume fraction is supposed to vary continuously in space and time. Conservation equations for each phase (Navier–Stokes equations) together with physical constitutive relations (usually from experimental correlations) and a partial differential equation for the evolution of the volume fraction are posed. The solution of this set of equations describes the evolution of the flow.

Different levels of complexity can be found to describe the EE models. Among the simplest is the Volume of Fluid (VOF) model [20], which defines a single set of momentum equations shared by all phases, while the volume fraction is tracked throughout the domain following the convective equation, $\partial\alpha\partial T+u\cdot\nabla\alpha$

$$\frac{\partial \alpha}{\partial t} + \mathbf{u} \cdot \nabla \alpha = 0$$

being u the common phase velocity. A similar approach is followed by phase field methods [21], where a phase-field parameter which identifies each phase is defined. The evolution of this parameter is modelled through a partial different equation with more physical meaning than in VOF, see e.g. Canh–Hilliard equation. More complex models consider that each of the phases is described by its density, velocity, temperature, and pressure (see for example the Baer and Nunziato model [22-29]). These models are usually closed with mathematical relations for the interaction between the phases (e.g. drag or pressure relaxation).

A different approach is followed by the EL methods which consider that only one of the phases is continuous (Euler) while the other/s is/are dispersed (Lagrange). The continuous Navier–Stokes equations are solved for the Euler phase while the Lagrange particles are tracked (individually or as groups) [30]. Lagrange particles are used to represent objects that fall under the resolution level of the numerical grid. Liquid droplets are one of the most common examples. Two different levels of coupling between the Euler and Lagrange phases are usually considered. In the one–way coupling, the dispersed phase is transported by the continuous phase but the latter is not affected by the former. The two–way coupling also considered the

effect of the Lagrange into the Euler phase. This is the reference model to simulate extinction problems [31] and specifically water mist [32].

It addition to that there are multiphase models specially developed to simulate the atomization problem. For example, the Σ-Y model [33, 34] is an EE that treats the mixture as a fluid with a single velocity field. Under the assumptions of high Reynolds and Weber numbers, it separates large–scale flow features (mass transport) from small–scale flow features (atomization). Both the evolution of the liquid fraction, Y and the density of the interphase surface area, Σ, (that accounts for the small–scale atomization) are modelled by transport equation.

3.2 A note on the phase change process

Two different scenarios might be considered for phase–change: first, if the liquid temperature is above its boiling temperature (T_b) at a given pressure, the liquid will boil provided that the system temperature remains higher than its boiling temperature. Second, for multicomponent systems (in this case fire extinction agent and air) phase change can exist even if $T < T_b$. In this case, the liquid evaporates (and also part of the surrounding gas condensates) until the chemical equilibrium is fulfilled (equal fugacities or chemical potentials for both phases). At moderate pressures, this equilibrium is usually approximated by the Clausius–Clapeyron and Raoult's law. In this particular problem, it would be interesting in the second scenario, so the phase change is driven by the chemical equilibrium between the components.

3.3 Two-phase flow numerical methods

Any numerical methodology consists of a model and a solution procedure. A model is a mathematical representation of the physical process to be predicted or simulated. Models usually neglect some less important or less influential phenomena [36].

Keeping in mind that ANSYS–Fluent will be used as a simulation tool at an industrial level, a quick review of the most relevant EE and EL models currently implemented in ANSYS– Fluent is given here. A more detailed description of the models implemented in ANSYS– Fluent can be found in [38].

Three EE models are implemented in ANSYS–Fluent, in order of increasing accuracy and complexity they are: VOF, Mixture and Eulerian. VOF is recommended if enough resolution to track interfaces is available. It should be mentioned that the VOF model may present problems (inaccuracies or convergence issues) where large velocity, temperature or viscosity differences exist between the phases. Mixture and Eulerian models are recommended for bubbly, droplet or particle-laden flows in which volume fraction exceeds 10%. The mixture model permits different velocities for each phase while the Eulerian model solves continuity, momentum, and energy for each of the phases. As a result, the Eulerian model is more accurate and requires more computational effort than Mixture model. The complexity of the Eulerian model can make it less computationally stable than the mixture model. Finally, Euler–Lagrange (discrete model) is also implemented in ANSYS–Fluent. It is recommended for flows in which phases mix is below 10%.

As a result (see Table 2), it can be inferred that VOF model should be used when enough resolution to capture interfaces is available, Mixture or Eulerian model should be used if there is not enough resolution to capture interfaces but volume fraction exceed 10% and EL approach should be used if the volumetric phase mix is below 10%.

	VOF	Mixture/Euler	Euler-Lagrange
Volume fraction	α >> 0.1	α > 0.1	α < 0.1

Table 2 Multiphase models included in ANSYS–Fluent.

In the problem the initial condition of our problem is a pressurized vessel that discharges the fire extinction agent through an atomizer to the ambient. This is a two-phase problem, e.g. phase 1 is the gas (air + vapor of fire extinction agent) and phase 2 is the fire extinction agent in liquid form. If we focus in the early stages of the process, i.e. before the fire extinction agent is completely atomized, the interfaces may be tracked and therefore a EE–VOF approach might be usable. However, after the fire extinction agent is atomized, the tracking of the interfaces becomes prohibitively expensive due to the expected droplets sizes (diameters of ~ μm based on semi-empirical correlations and preliminary one–dimensional results). Furthermore, the nature of the phase–change (highly dependent on the droplet sizes) makes the EL method a well-suited approach. In the following sections, we describe the EE–VOF and the EL approach available in ANSYS–Fluent.

3.4 Euler–Euler (VOF)

VOF model describe in ANSYS–Fluent. The model considers an equation for the conservation of liquid volume fraction, global momentum and energy. Velocity, pressure, and temperature are considered uniform between phases. For the sake of clarity, we will limit the explanation of the VOF model to the two-phase system. We will assume that gas is phase 1 while the liquid is phase 2. Terms related to the phase change are included in VOF equations in red.

The transport of the volume fraction of phase 1 follows the VOF equation,

$$\frac{1}{\rho_1}\left[\frac{\partial(\alpha_1\rho_1)}{\partial t} + \nabla\cdot(\alpha_1\rho_1\mathbf{u}) = \dot{m}'''_{21}\right]$$

where ρ1 is the phase 1 density, u the common velocity vector. The phase 2 volume fraction can be computed as $\alpha_2 = 1-\alpha_1$. The term m_{21} accounts for mass transfer from phase 2 to phase 1, volumetric phase change rate (kg/(m^{3}s)).

A common momentum equation for both phases is defined:

$$\frac{\partial(\rho\mathbf{u})}{\partial t} + \nabla\cdot\rho\mathbf{u}\mathbf{u} + \nabla p = \rho\mathbf{g} + \mathbf{F}_{vol} + \nabla\cdot\left[\mu(\nabla\mathbf{u} + \nabla\mathbf{u}^T)\right]$$

where p is the pressure (obtained from the incompressibility condition $\nabla \cdot u = 0$), $\rho = \alpha^1\rho^1 + \alpha^2\rho^2$ is the common density, $\mu = \alpha^1\mu^1 + \alpha^2\mu^2$ is the common viscosity, g is the gravitational acceleration and Fvol accounts for the volumetric force due to surface tension. For the problem considered here (Re>> 1, We>> 1) surface tension effects are negligible. However, if required, they can be computed using several techniques (Continuum Surface Stress - CSS or Continuum Surface Force - CSF), see [26] for details.

3.5 Euler–Lagrange

In the Euler–Lagrange approximation the ambient gas is solved following a Eulerian description while the liquid, assumed to be dispersed, is tracked as individual droplets. This model is only valid to simulate the flow outside the atomizer (after the fire extinction agent has been atomized), therefore a valid inflow boundary condition should be provided. Several models to compute the inflow boundary condition are implemented in ANSYS–Fluent. The explanation will be decomposed into two parts. First, we will explain the modifications required in the Euler solver to take into account the Lagrangian (drops) part. Second, we will review the equations that model the evolution of each of the droplets. The model described here follows the user guide of NIST-FDS (Fire Dynamic Simulator) [31, 27]. This solver is chosen as it specifically designed for this problem. The main differences (they are minor) with ANSYS–Fluent's model will be highlighted and will be included in ANSYS–Fluent if required.

Euler solver

Momentum equation:

$$\frac{\partial(\rho\mathbf{u})}{\partial t} + \nabla \cdot \rho\mathbf{u}\mathbf{u} + \nabla p = \mathbf{f}_b + \rho\mathbf{g} + \nabla \cdot \left[\mu(\nabla\mathbf{u} + \nabla\mathbf{u}^T)\right]$$

where now ρ refers to the gas density and u its velocity, p is the pressure (obtained from the incompressibility condition $\nabla \cdot u = 0$), fb represents the momentum transferred from particles to the gas (see below for the definition), μ is the gas viscosity and g is the gravitational acceleration.

Energy equation:

$$\frac{\partial(\rho E)}{\partial t} + \nabla \cdot [\mathbf{u}(\rho E + p)] = \nabla \cdot [k\nabla T] + q_b$$

where energy E is based on the specific heat and the temperature T, k is the thermal conductivity and q_b represents the energy transferred from the particles to the gas.

Lagrange solver

For Lagrange solver, it is important to notice that, to address computational efficiency, not every droplet is tracked as the computational effort would be too high. Instead, a smaller number of "super droplets" or parcels are tracked, where each super droplet represents many

individual real droplets with the same diameter and thermophysical properties [31]. This approach leads to extremely high rates of heat and mass transfer as very fine droplets require a large super droplet weighting factor. The weighting factor is omitted here for the sake of simplicity.

The momentum equation of the particles reads the particle velocity by:

$$\frac{d\mathbf{u}_p}{dt} = \mathbf{g} - \frac{1}{2}\frac{\rho C_d A_{p,c}}{m_p}(\mathbf{u}_p - \mathbf{u})|\mathbf{u}_p - \mathbf{u}|$$

where u_p is the particle velocity, g the gravity, C_d its drag coefficient (the function of its Reynolds number), $A_{p,c}$ the particle cross-sectional area and m_p the particle mass. Gas velocity u, and gas density, ρ, are obtained from the Euler part of the solver. The momentum equation solved by ANSYS–Fluent takes into account buoyancy effects, which are negligible for liquid droplets moving through the air. Being the velocity of the particles known, the particle position x_p, is determined from the equation:

$$\frac{d\mathbf{x}_p}{dt} = \mathbf{u}_p$$

Based on a sphere, the drag coefficient is computed as:

$$C_d = \begin{cases} 24/Re_D & Re_D < 1 \\ 24(0.85 + 0.15Re_D^{0.687})/Re_D & 1 < Re_D < 1000 \\ 0.44 & 1000 > Re_D \end{cases}$$

With

$$Re_D = \frac{\rho|\mathbf{u}_p - \mathbf{u}|2r_p}{\mu(T)}$$

where μ(T) is the dynamic viscosity of air at temperature T and r_p the particle radius. Alternatively, the correlation Brown and Lawler correlation for Cd [4] is supposed to be valid for $Re_D < 2\times105$:

$$C_d = \frac{24}{\mathrm{Re_D}}(1 + 0.15\mathrm{Re_D}^{0.681}) + \frac{0.407}{1 + \frac{8710}{\mathrm{Re_D}}}$$

Additional models to compute de drag coefficient can be found in [31, 28]. For example, ANSYS–Fluent uses the Morsi and Alexander [38] model for spherical particles:

$$C_d = a_1 + \frac{a_2}{\mathrm{Re_D}} + \frac{a_3}{\mathrm{Re_D^2}}$$

where a_1, a_2 and a_3 are constants that apply over several ranges of Re_D given in the appendix of [38]. These models give similar values for the drag coefficient as can be seen in Fig. 5.

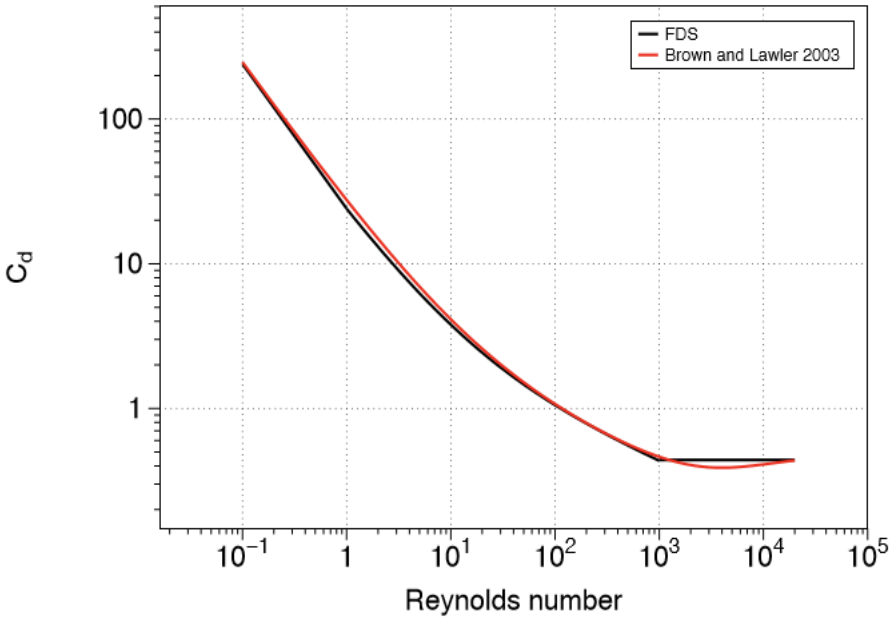

Figure 5 Comparison of drag coefficient for a sphere implemented in FDS and Brown and Lawler correlation

By summing the forces transferred from each particle in a grid cell and dividing by the cell volume V, the momentum transferred from particles to the gas,

$$\mathbf{f}_b = \frac{1}{V}\sum\left[\frac{\rho}{2}C_d A_{p,c}(\mathbf{u}_p - \mathbf{u})|\mathbf{u}_p - \mathbf{u}| - \frac{dm_p}{dt}(\mathbf{u}_p - \mathbf{u})\right]$$

It should be noticed that ANSYS–Fluent does not take into account the change of momentum due to the evaporation of the droplets.

Energy

The mass and energy transfer can be described by the following set of equations

$$\frac{dT_p}{dt} = \frac{1}{m_p c_p}\left[\dot{q}_r + A_{p,s}k_h(T - T_p) + \frac{dm_p}{dt}h_v\right]$$

Here, m_p is the mass of the droplet, $A_{p,s}$ the surface area of the liquid droplet, km the mass transfer coefficient (to be discussed below), ρ the gas density, c_p the liquid specific heat, k_h the heat transfer coefficient between the droplet, the gas and h_v the latent heat.

3.6 Turbulence Modeling approaches for simulation

Nowadays, the use of computational models to predict the spray behaviour is of vital importance due to the fact that different solutions or configurations can be evaluated without using an expensive physical facility. A primary classification of these models, attending to their complexity, divides them into two groups: thermodynamic and fluid-dynamic models.

Thermodynamic models are useful to have a fast-initial estimation, but fluid-dynamic models are completer and more accurate. The fundamentals are the resolution of a set of equations that govern the flow (continuity, momentum, energy, etc.). Due to the complex problem to solve, it is necessary to make use of the computational fluid dynamics (CFD) environment with all their numerical algorithms for discretization and resolution.

Turbulence flow regimes, in contrast with laminar flow regimes, are characterized by velocity and pressure fluctuations and the presence of eddies with many different scales. Turbulence is maintained through an energy transfer process, namely energy cascade, that occurs from the most energetic eddies to the smallest ones. Energy is dissipated through viscosity effects when reaching the smallest eddy scales. This process is known as the theory of energy cascade of Kolmogorov [45]. The higher the Reynolds number, the greater the range of scales.

Numerical treatment of turbulent flow is a characteristic or parameter of each CFD model and thus, it represents a first method of classification

Direct Numerical Simulation (DNS):

The first option describes the turbulent flow without using any model, i.e. turbulent flow equations are directly solved. however, a numerical mesh fine enough to resolve all turbulent length scales is mandatory together with small time steps. As a result, the huge computational cost of this methodology (increases with Reynolds number Re) for current computing power is the greatest drawback. Due to this fact, its application remains outside the industrial level and it is only adopted in simple, academic cases in which gives support to fundamental research.

Large Eddy Simulation (LES):

The second type of numerical approach of turbulence is a compromise between the direct resolution and the modelling. Large scales of the turbulent flow are directly resolved whereas the smallest scales of the turbulent flow are modelled. An important consequence of that is the great reduction of the computational cost. The cell size of the calculation mesh is usually the determining factor of what scales may be resolved (spatial filtering) and the effect of the modelled scales on the resolved ones is taken into account by the subgrid-scale model. Many structural details of the turbulent flow can be retained with this approach. This is the main reason for the increasing use of this methodology, even at the industrial level recently.

However, a significant issue is that several LES simulations have to be done of the same problem to obtain statistically significant mean values to compare with experimental data.

Reynolds Average Navier-Stokes (RANS):

RANS computations are the last methodology, in which the whole range of turbulent scales is modelled. Equations for the mean values of the flow are solved, which are obtained by Reynolds (or Favre) averaging the instantaneous balance equations. Computational cost is relatively low even for large and complex problems, hence being still the most widely used approach for CFD simulations. The disadvantage of RANS is that new unknowns arise during the averaging process that makes it necessary to solve additional equations to overcome this closure problem. For this purpose, a variety of turbulence models have been developed with the attempt to best describe the effect of turbulent motion.

For numerical simulation of primary atomization, three approaches can be used which are described previously, i.e. DNS, RANS or LES. As in the turbulent flow of a single-phase fluid, multiphase flows possess a large range of scales, ranging from the size of the smallest dispersed phase structure to the size of the system under investigation. In the primary atomization process, the thickness of ligaments and droplets that follows the break-up of the interface can be smaller than the Kolmogorov length scale. DNS of such flows without any modelling of the two phases aspect is thus not affordable. Two-fluid models may be used for DNS of two-phase flows, showing low Reynolds number. Boeck et al. [31] used VOF for full numerical simulations of two-phase liquid-gas sheared layers, intending to study atomization. One of the first DNS of primary atomization was performed by Menard et al. [32], with an LES methodology coupled with VOF (CLSVOF), to study the primary break-up process. The purpose of these previous works is to study physical phenomena in primary atomization and to serve as a reference for validating other modelling approaches, as RANS and LES models. Nevertheless, they involve a quite small area, limited by a few injector diameters in the downstream direction. Simulating the whole atomization process going until several hundred of diameters in the downstream direction is hardly feasible with DNS.

Industrial approach uses the RANS system with Euler-Lagrange models: Eulerian for the gas phase associated with a Lagrangian solver "reproducing" the presence of physical particles inside the domain [38]. Based on a wrong hypothesis considering models for non-dense flow at the injection, correct results can be obtained thanks to the convective characteristics of the Lagrangian method. Even though the provided results are rough, this approach has been widely adopted because of its ability to model the whole spray, from the nozzle outlet to the mixing area inside the domain, even if the flow is inaccurate at the nozzle outlet. Some RANS turbulence models which are available in Fluent are listed below.

Spalart-Allmaras Model

This model is relatively one equation model. It was designed specifically for aerospace applications and turbomachinery applications [39]. It is more effective for a low Reynolds-number model. In FLUENT, this model has been implemented to use wall functions when the mesh resolution is not sufficiently fine. This model is less sensitive to numerical error when non-layered meshes are used near walls. However, it is still relatively new, and no claim is made regarding its suitability to all types of complex engineering flows.

Standard $k-\varepsilon$ Model

It is a simplest two equation turbulence model in which the solution of two transport equations allows the turbulence velocity and length scales to be independently determined. The standard $k-\varepsilon$ model in FLUENT use for practical engineering flow calculations in the time since proposed by Lauder and Spalding [40]. This model is popular in industrial flow and heat transfer simulation due to robustness, economy, and reasonable accuracy for a wide range of turbulent flows. Also, this model gets improve to increase the performance. Two of these variants are available in FLUENT: the RNG $k-\varepsilon$ model [41] and the realizable $k-\varepsilon$ model [42].

RNG k – e model

The RNG $k-\varepsilon$ model was derived using a renormalization group theory. It is similar form of the standard $k-\varepsilon$ model but includes some refinements. This model has an additional term in e equation which helps to improve the accuracy of rapidly strained flows. It also includes the effect of swirl turbulence. While the standard $k-\varepsilon$ model is using for high Reynolds number model, the RNG $k-\varepsilon$ model is also validated for low Reynolds number. However, it depends on an appropriate treatment of near wall region.

Realizable $k-\varepsilon$ Model

This model is containing a new formulation for the turbulent viscosity compare to standard k e model. A new transport equation for the dissipation rate is included which is derived from the transport of the mean square vorticity fluctuation. It satisfies certain mathematical constraints on the Reynolds stresses, consistent with the physics of turbulent flows. It predicts accurately the spreading of both planar and round jets. It gives good performance for flows involving rotation, boundary layers under strong adverse pressure gradients, separation and recirculation. Recent studies shown that this model provides the best performance of all $k-\varepsilon$ version for several validations of separated flows and flows with complex secondary flow features. One of the limitations of this model is that it produces nonphysical turbulent viscosities in situations when the computational domain contains both rotating and stationary fluid zones.

Standard $k-\omega$ Model

The standard k-ω model in FLUENT is based on the Wilcox $k-\omega$ model [43]. It is an incorporates modifications for low-Reynolds-number effects, compressibility and shear flow spreading. The Wilcox model predicts free shear flow spreading rates that are in close agreement for mixing layer and plane, round and radial jets. It is applicable to wall bounded flows and free shear flows. More advance of this model is also available in FLUENT called the SST $k-\omega$ model.

Shear-Stress Transport (SST) $k-\omega$ Model

This model was developed by Menter [44] to increase the accuracy of the model in the near-wall region with the free-stream independence of the $k-\omega$ model in the far field. It is similar to the standard $k-\omega$ model but includes some refinements. Both models are multiplied by a blending functions and added together. The blending functions is designed like in that way that the standard $k-\omega$ model activates for wall region and the transformed $k-\varepsilon$ model for away from the surface. The modelling constant are different. In general, SST $k-\omega$ model more accurate and reliable for a wider class of flows (e.g., adverse pressure gradient flows, airfoils, transonic shock waves) than the standard $k-\omega$ model. Therefore, this model suits very well for this problem.

3.7 Secondary Break-up models in ANSYS Fluent

Among all the sub-models employed in Eulerian-Lagrangian methods (which are the liquid injection model, the spray breakup model, the droplet drag, collision, and turbulent dispersion models, the droplet/wall interaction model, and the evaporation model) the break-up one is the most important. There are several options for this model depending on the main atomization mechanism:

Kelvin-Helmholtz or wave break-up model based on a liquid jet stability analysis: it is described in detail by Reitz [45]. The analysis considers the stability of a cylindrical, viscous, liquid jet issuing from a circular orifice into a stagnant, incompressible, inviscid gas. The primary breakup of the jet is then related to the Kelvin-Helmholtz instability induced by the relative velocity at the interface. Among the many wavelengths, the one which grows faster is considered as the one responsible for the break-up.

Kelvin-Helmholtz ACT break-up model developed by Som and Aggarwal [46]: It is a modification of the Kelvin-Helmholtz model that includes the effects of aerodynamics, cavitation, and turbulence on the primary breakup.

Rayleigh-Taylor break-up model: In addition to the Kelvin-Helmholtz break-up model, the Rayleigh-Taylor instability is also believed to be responsible for droplet break-up[47]. The unstable Rayleigh-Taylor waves are thought to occur due to the rapid deceleration of the droplets from the magnitude of the drag force.

Taylor Analogy Break-up model developed by O'Rourke and Amsden [48]: It is a classic method for calculating drop distortion and break-up. This method is based on Taylor's analogy between an oscillating and distorting droplet and a spring-mass system.

Linearized Instability Sheet Atomization model developed by Senecal et al. [49]: It includes two parts, a general liquid sheet break-up mechanism proposed by Dombrowski and Johns [49] and a liquid injection methodology specifically for pressure-swirl atomizers.

Reitz and Diwakar model: According to this model, droplet break-up due to aerodynamic forces occurs in one of the following modes bag break-up in which the non-uniform pressure field around the droplet causes it to expand in the low-pressure wake region and eventually disintegrates when surface tension forces are overcome, and sheet stripping break-up in which liquid is sheared or stripped from the droplet surface [50].

Pilch and Erdman model: Droplet break-up is directly calculated from correlations developed by Pilch and Erdman [51] who assumed that it occurs if the droplet Weber number is greater than the critical Weber number.

Hsiang and Faeth model developed by Hsiang and Faeth [52]: It is valid for droplet Weber numbers lower than 1000 and covers all types of break-ups that are of interest in Diesel engines spray applications.

Chu model developed by Chu and Corradini [53]: It is based on the Rayleigh-Taylor instabilities. Its theoretical correlation predicts droplet sizes based on an exponential function.

Kelvin-Helmholtz Rayleigh-Taylor model described by Patterson and Reitz [54]: It consists of a composite process that Kelvin-Helmholtz aerodynamic instabilities growing on a droplet surface are simultaneously calculated with Rayleigh-Taylor instabilities resulting from the deceleration of the injected droplets. The two physical models compete with each other and the one predicting the fastest onset of instability gives rise to break-up events.

Chapter 4

4 Experimental Setup

4.1 Setup description

A large constant pressure constant volume vessel was designed and assembled to test two new alternatives for replacing Halon 1301 in the fire suppression systems on aircraft cargo cabin. A sketch of the complete test rig is depicted in Figure 6. A pressurized container is used to set the injection pressure (upstream pressure). A 20 MPa pressurized nitrogen bottle is connected to the container and, using a manual valve, allows increasing or decreasing the pressure of the container. Before pressurizing, the container is partially filled up with the fire suppression agent (either water or Novec 1230). This container is directly connected to the nozzle with a pipe of 10mm inner diameter, and a manual ball-type valve controls de injection. Manometers are used in all deposits and containers to monitor the pressure, as well as thermocouples to monitor the temperature. A piezoelectric Kistler pressure sensor (SN 2144942/2013) is located at the pipe just upstream of the nozzle. This pressure signal is utilized to measure the injected mass flow rate and therefore the total injected mass.

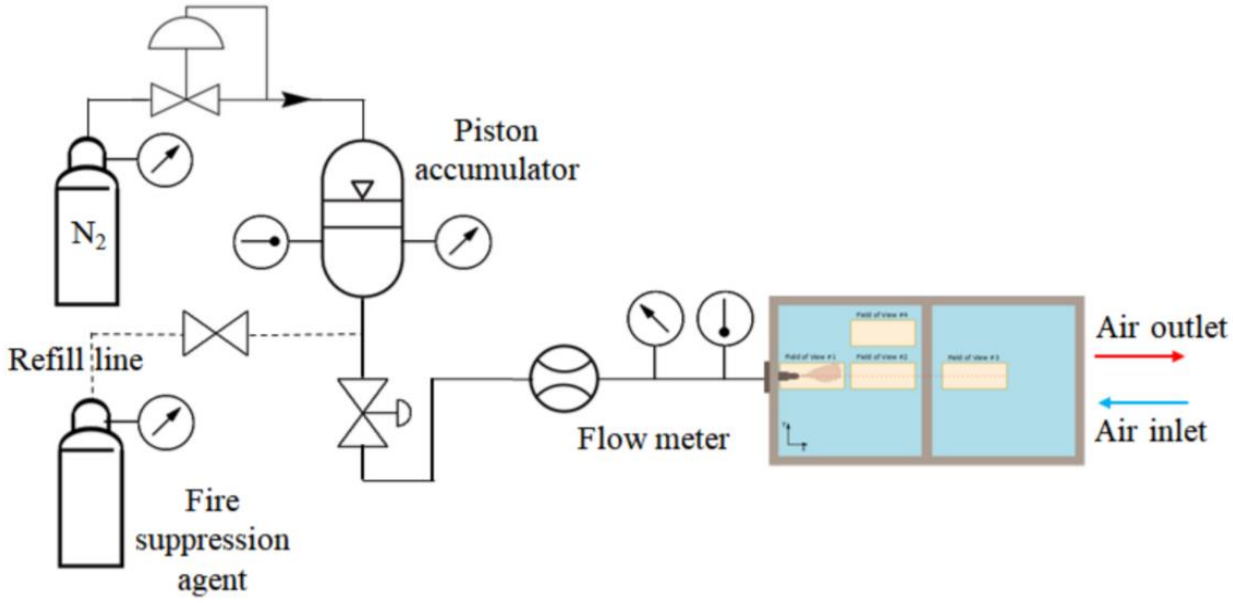

Figure 6 Diagram of injection system

Optical instruments utilized in the measurements do not allow to record the whole field of view of 750×1500 mm. Therefore, three different positions are selected as fields of view, as already depicted in Figure 6. Two Measurements techniques are used to visualize the shape of the spray: 1) Diffuse Backlight Illumination (DBI) 2) Schlieren technique

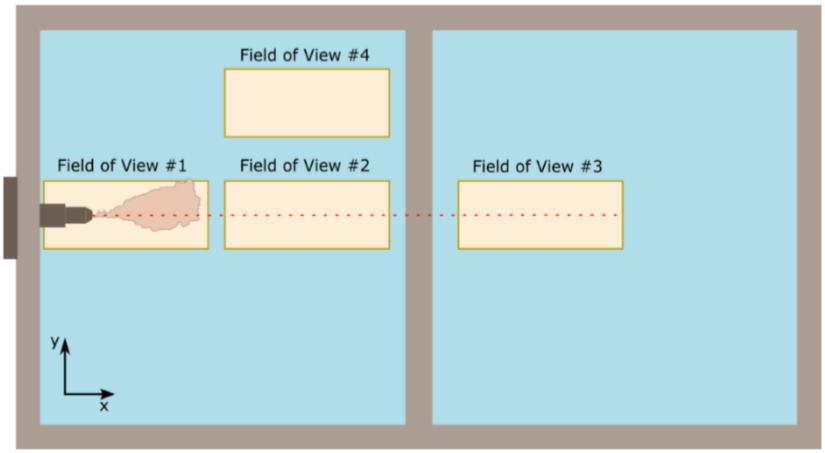

Figure 7 Schematic diagram of the side view of the vessel

4.2 Nozzles

To simplify the test rig and the following Computational Fluid Dynamics (CFD) validation, a nozzle with a single orifice oriented in the axial direction has been manufactured. A drawing with the main dimensions and a picture of the nozzle are represented in Annex.

Based on the previously obtained results Novec 1230 was not enough to reach the maximum possible volume with the actual nozzle geometry used for the experimental campaign. Due to that, geometrical changes to the nozzle are necessary to improve the atomization. Therefore, instead of a different fire suppression agent, it is decided to carry out the new experimental campaign with a new nozzle that promotes atomization. The new nozzle of Spraying Systems Co. ref. 1/4GG-SS3009, shown in Annex, is selected. It has the same orifice outlet diameter of 2 mm (to accomplish with the flow rate requirements) but includes a swirler to add a tangential component to the flow and so improve spray atomization and increase spray angles.

4.3 Working fluids

The two fire suppressant alternative fluids being tested are water and Novec1230. Their main thermo-physical properties are listed in Table 2 [10, 11] in comparison to those of Halon 1301 (agent to be replaced).

Property	Halon1301	Novec1230	Water
Chemical formula	CF_3Br	$C_6F_{12}O$	H_2O
Molecular weight [g/mol]	148.91	316.04	18.02
Boiling point at 0.1 MPa [K]	215.35	322.35	373.15
Freezing point [K]	105.15	165.15	273.15
Vapor pressure [MPa]	1.47	0.002	0.04
Density [kg/m3]	1551	1616	1000
Liquid viscosity [kg/(m·s)]	1.60E-04	3.90E-04	1.03E-03
Surface tension [N/m]	5.95E-03	1.08E-03	7.28E-02

Table 2 Thermo-physical properties of Halon 1301 and the alternative suppressants. All values are at 298 K

4.4 Test matrix

To cover all possible scenarios, three different values of injection pressure are tested. The complete final test matrix is summarized in Annex.

4.5 Experimental results

Mass flow rate, injection pressure, spray penetration, and cone angle are measured at three visualization windows located at different axial positions. Example, the mass flow rate curves calculated for one condition for water and Novec1230 showed in figure 8. Mass flow rate of Novec1230 is higher than water due to high density

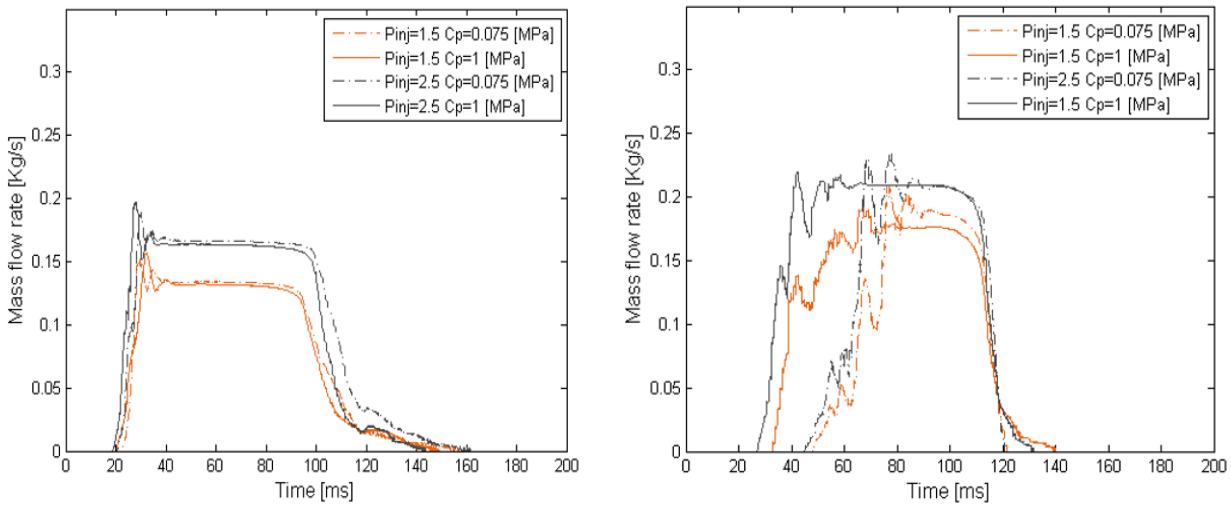

Figure 8 Water and Novec1230 mass flow rate

Figure 9 shows the entire spray penetration development for water along all the fields of views, the red box indicates the field of view near to the nozzle exit and it is highlighted only because that position is taken into account to analyse the effects injection conditions in the spray penetration curves. It can be noticed that higher injection pressure leads to faster spray penetration [33]. The shape of the curve changes from a parabolic trend to a straight line because in the first moments of the injection process the spray accelerates as it is injected. Later, the spray reaches the steady-state in which the pressure stabilize the spray speed is constant [34].

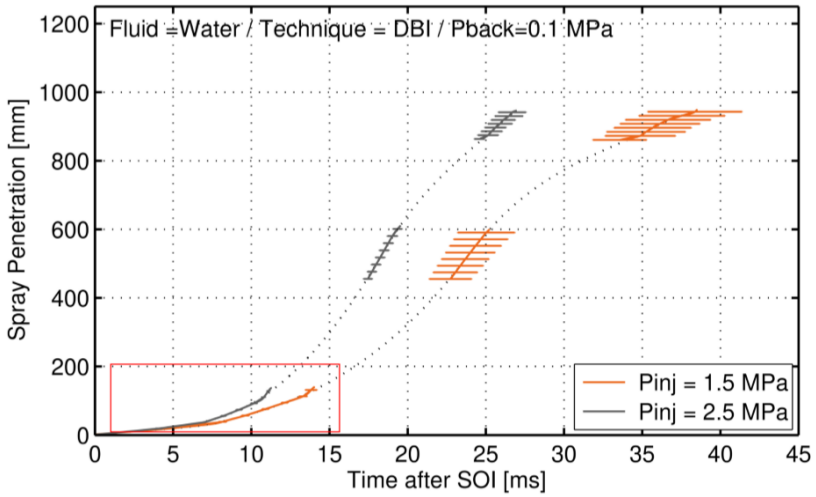

Figure 9 Water liquid spray penetration along all the fields of views obtained

4.6 Spray angle

Both nozzles have the same outlet diameter the only difference is that the new nozzle has an internal piece that works as swirler that as said by Amini [36] induces the work fluid to pass under pressure through the tangential ports of the internal geometry of the nozzle to develop a free vortex in the swirl chamber of the nozzle. Figure 10 shows the mean spray cone angle for both nozzles. It is observed that the higher the temperature and the lower the backpressure, the wider the spray angle is obtained. The effect of the injection pressure on the spray angle is small and depends on the particular geometry of the nozzle [35]. For the case study, an average spray angle of 25-30º was obtained for all conditions coinciding with what was reported by the manufacturer.

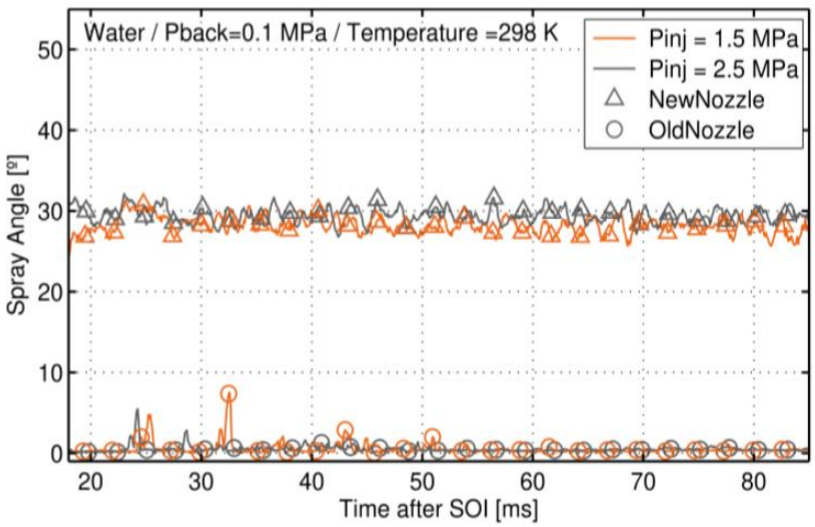

Figure 10 Steady state spray angle comparison between nozzles.

Chapter 5

5 2D E-E VOF Model

5.1 Geometry & Boundary Condition

Geometry and boundary conditions of 2D domain are present in Figure 11 which is representation of experimental setup of nozzle 1. As this is axis-symmetric model, A first approximation to this sort of problem is to perform 2D simulation, of course Real experimental setups are always 3D, but, as a first approximation to the real problem, 2D simulation can reasonably for this type of problem to reduce computational cost.

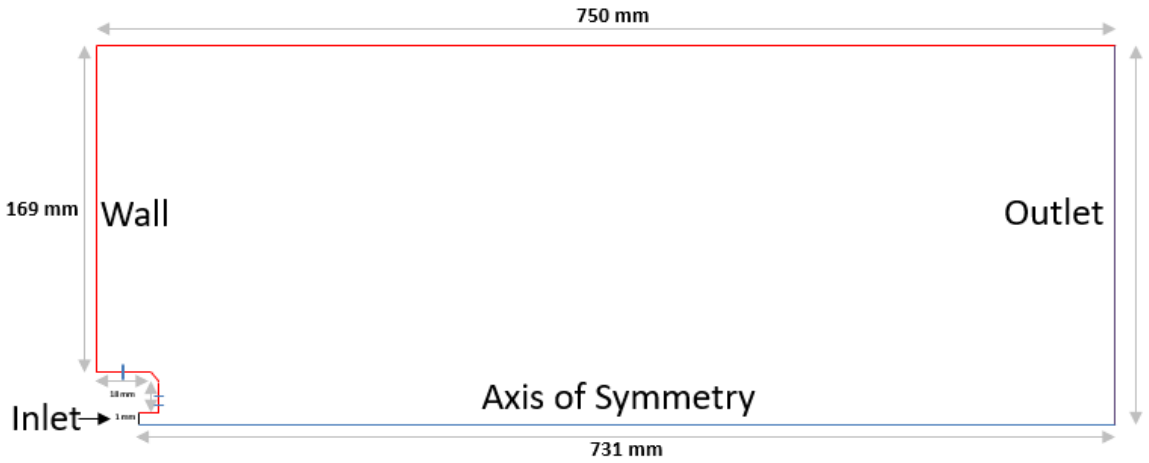

Figure 11 Dimensions for the 2D CFD domain

Figure 12 shows time evolution of the mass flow rate obtained from experimental facilities that used as inlet boundary condition for both substances, water and Novec 1230.The average value of all repetitions and all positions for each test condition is used together with the standard deviation of the measurements

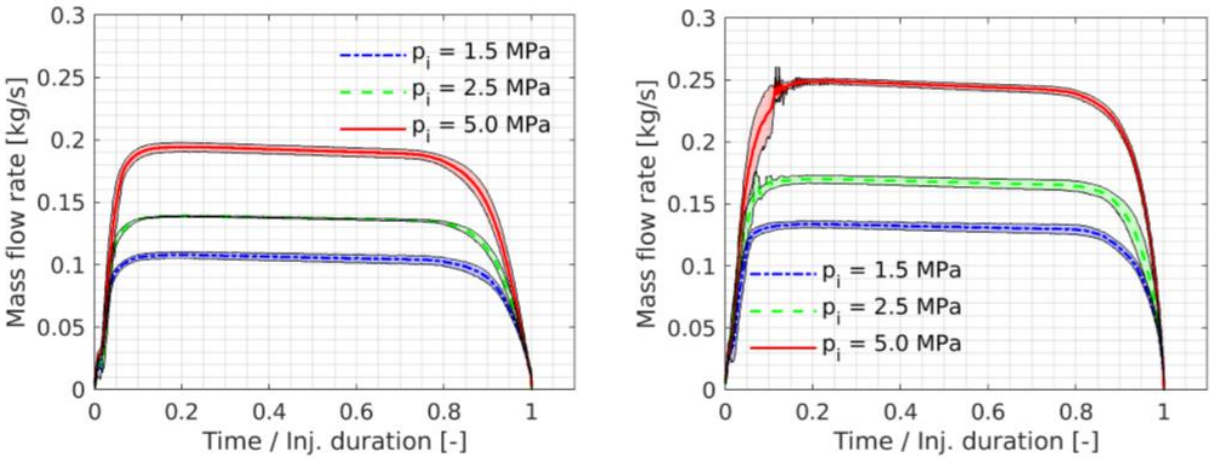

Figure 12 Time evolution of the averaged mass flow rate during the suppressant injection event

5.2 Numerics

Table 3 lists the numerical settings and methods used most often in testing the present method in ANSYS Fluent.

Setting / model	
Solver	Pressure-based
Time	Transient
Multiphase model	Explicit VOF
Implicit Body Force	Yes
Surface Tension	Enable
Turbulence Model	SST k - omega
Pressure-Velocity coupling	Coupled
Global Courant Number	<1

Table 3 Numerical setting for simulation in ANSYS Fluent

5.3 Mesh independence study

Generally, the requirements for mesh structure are important at the nozzle to capture the spray characteristics and also mesh independence study can help us to determine the optimum point for accurate results without using high computation costs. So, we used three different values of mesh cells near nozzle which is shown in figure 13.

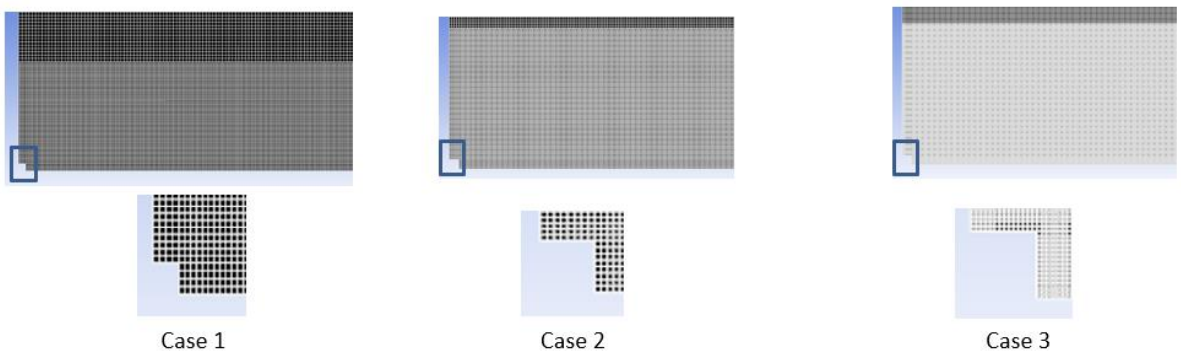

Figure 13 Number of cells at half nozzle

Case No	Number of cells at half nozzle	Total cells	Transient Time	Number of processor	CPU time (h)
1	4	0.17 million	15 ms	10	8
2	8	0.72 million	16 ms	10	23.6
3	16	1.5 million	16 ms	10	42.2

Table 4 Case matrix for mesh independence study

Figure 14 shows experimental penetration at 15 bar pressure is presented after time of injection to calibrate with the fluent results. There is not so much differences between case 2 and case 3 setups with experimental data in terms of penetration. Therefore, we choose case 2 mesh size for further simulation for other cases.

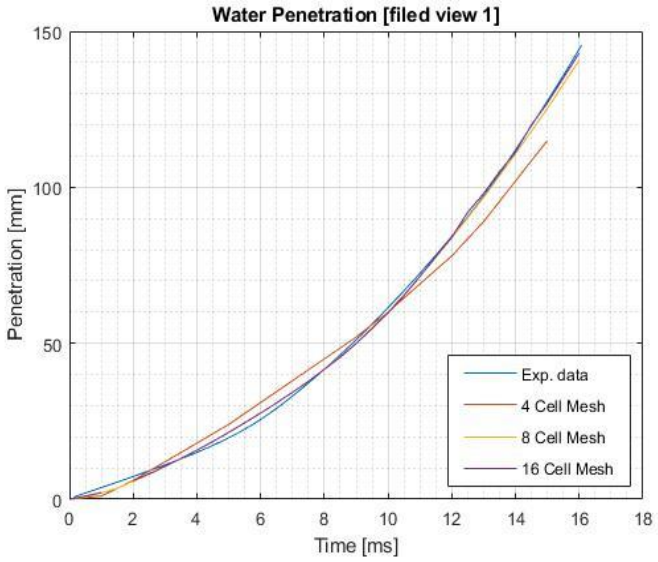

Figure 14 Penetration of water at 15 bar injection pressure

5.4 Validation

Figure 15 shows the spray penetration curves which we obtained from simulation for different injection pressure of two fluids and compare with experimental data. Water has higher spray velocity and so penetrates faster. This happens because the Novec1230 density is 1.6 time higher than water (which also defines the mass flow rate as shown in Figure 15). For both

fluids, as expected, higher injection pressure leads to an increase of the spray tip penetration [24].

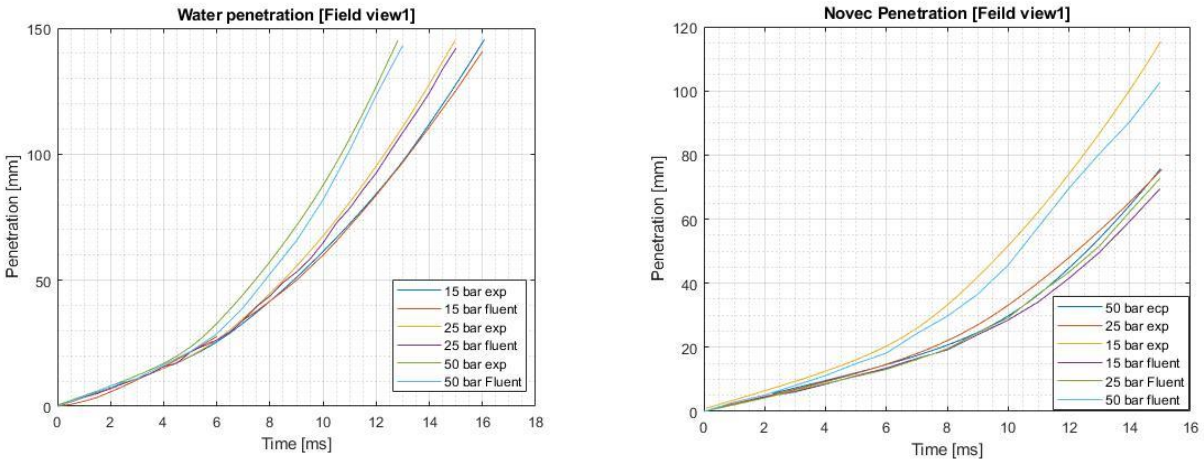

Figure 15 Penetration of water at different injection pressure bar

Nozzle 1 was intended for the injection of Halon 1301. Because of this, a poor performance was detected in the injection of Novec1230 so a new nozzle (Nozzle 2) of Spraying Systems Co Ref 1/4GG-SS3009 with the same outlet diameter and swirler was selected in order to add tangential component to the flow and improve spray atomization and increase cone spray angle. In this section we carried out internal flow characteristics of swirl nozzle (Nozzle 2).

Chapter 6

6 Internal flow study of atomizer nozzle

6.1 Geometric model and computational mesh

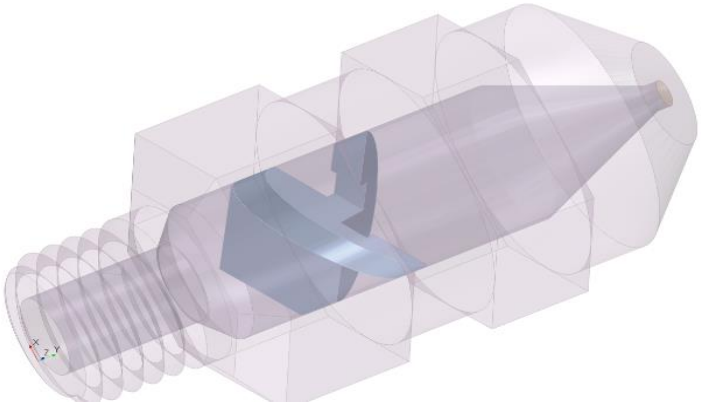

Figure 16 CAD model of Nozzle 2

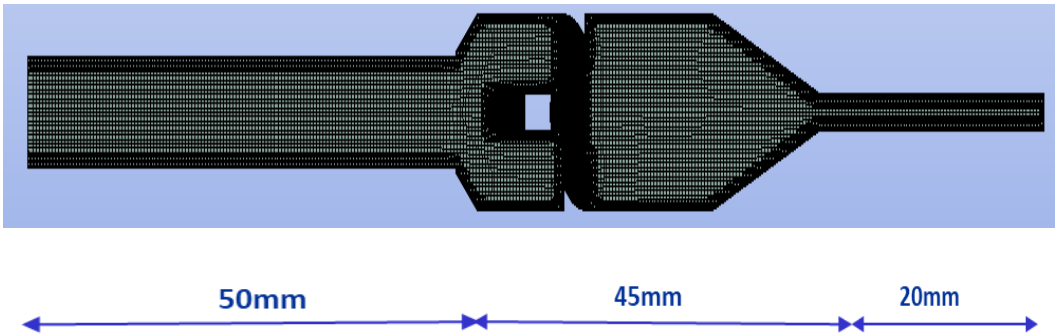

Figure 17 Meshing of nozzle 2

Simulation was performed in steady state, being the velocity inlet, considered as a condition of entry for injector for both fluids Water and Novec1230 and they are considered as incompressible. For all cases, the turbulent model employed was SST k – omega model which can predict very well far from the boundaries (wall) and near wall, a no-slip condition was adopted on the walls, and pressure outlet condition at exit of nozzle.

Case	Body cell size	Wall cell size	Elements [million]	Iteration	Time
#1	0.0009	0.00045	0.068264	500	0:17:15
#2	0.0008	0.0004	0.257518	500	0:32:15
#3	0.0007	0.00035	0.266037	500	0:35:48
#4	0.0006	0.0003	0.281427	500	0:39:48
#5	0.0005	0.00025	0.292311	500	0:45:57

Case	Body cell size	Wall cell size	Elements [million]	Iteration	Time
#6	0.0004	0.0002	1.149916	500	1:06:32
#7	0.0003	0.00015	1.292284	500	1:21:32
#8	0.0002	0.0001	5.340485	500	3:41:52
#9	0.0001	0.00003	13.225166	500	7:19:07
A (SC+)			0.257518		

Table 5 Computational cases

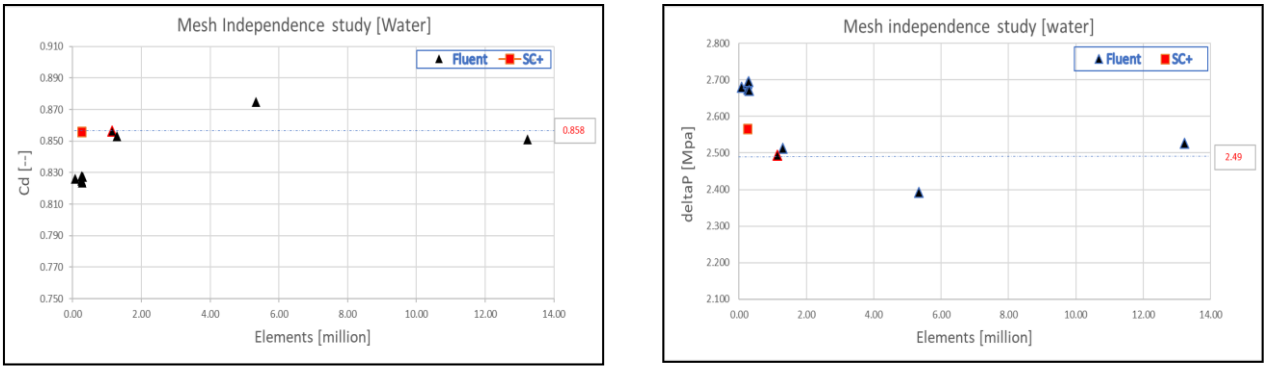

Figure 18 Mesh independence study results of water

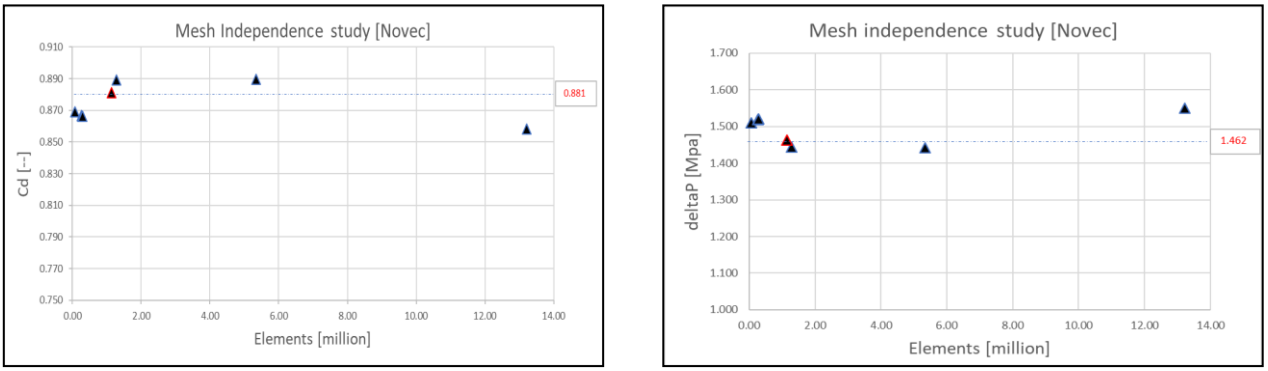

Figure 19 Mesh independence study results of Novec1230

6.2 Results

In Fig. 20 are shown the discrepancies of the results of the ‘‘Cd’’ numerical simulation for with respect to the manufacturer data sheet and Star C+ Simulation data. In the case of the results obtained numerically, a good approximation can be observed regarding the manufacturer data sheet.

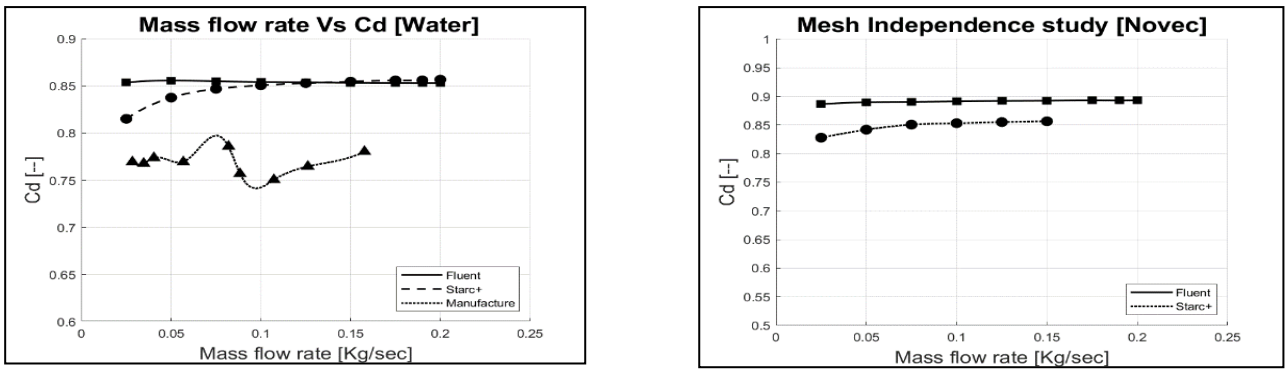

Figure 20 Comparison of co-efficient of discharge between fluent results and manufacture data for water and novec1230

Fig. 21 illustrates the changes in pressure difference as a function of mass flow rate to injector, the numerical simulation acquires a similar behaviour deviating slightly from the manufacture data sheet curve.

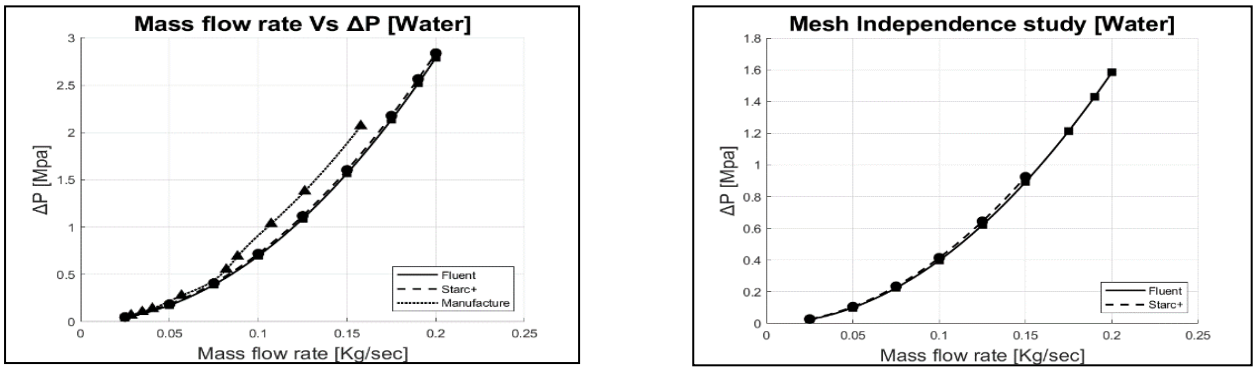

Figure 21 Comparison of pressure difference at inlet and outlet of nozzle between fluent results and manufacture data for water and novec1230

In Fig. 22 the spray angles obtained from numerical simulation are displayed. We see that the spray angle obtained with the simulation has reasonable approximation regarding the manufacture data sheet which claim max 30 degree, taking into account the different mass flow rate. However, on the other hand, the results of numerical simulation show a considerable deviation with respect to experimental data (17% approximately), this is due to limitations of the mesh in the interface. Figure 23 represents the mass flow rate obtained at nozzle outlet from simulation.

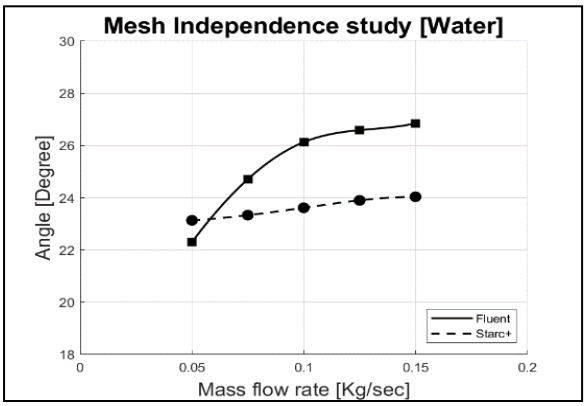

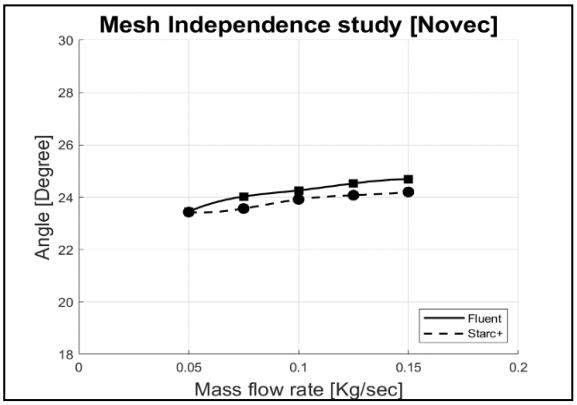

Figure 22 Penetration angle for nozzle 2

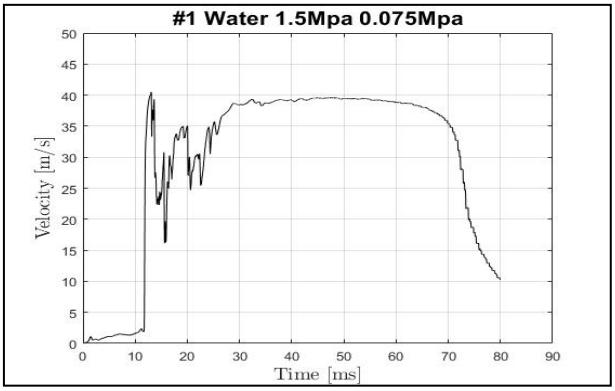

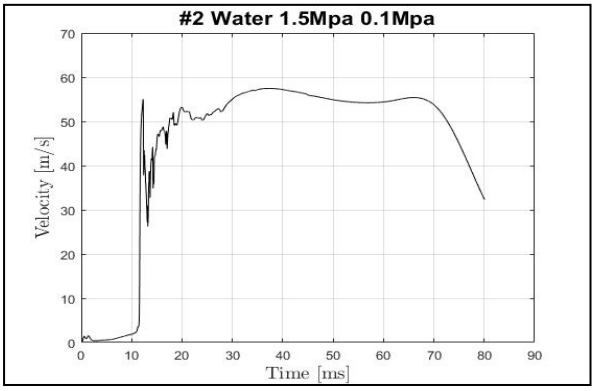

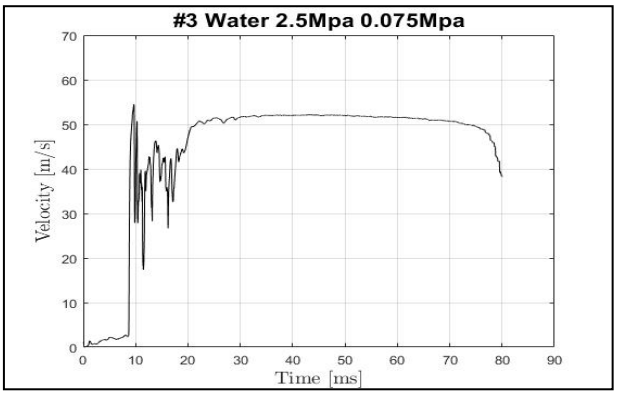

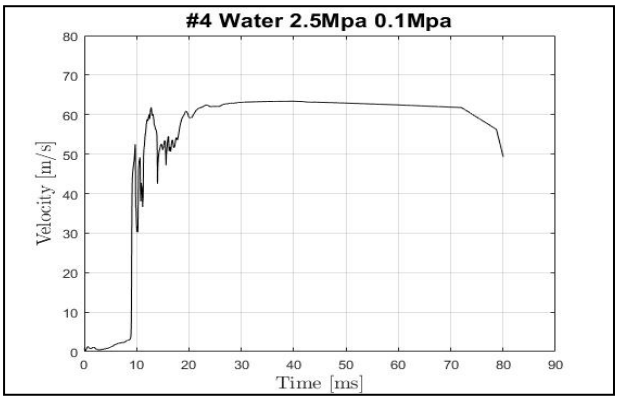

Figure 23 Mass flow rate at outlet of nozzle

Chapter 7

7 3D E-E Model

7.1 Geometry

The computational domain which is shown in figure represents injection test rig chamber of position 1. For this simulation only position 1 is taken into account to analyze spray penetration curves. The length of inlet pipe is incresed to 50 mm so it can matach with real test condition of experimental. The numerical setting used same as before used for 2D model.

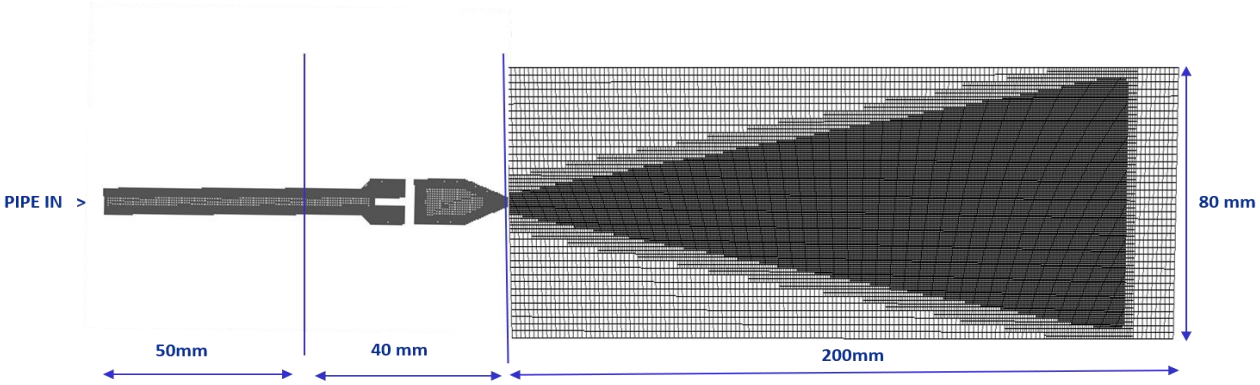

Figure 24 Dimensions of the 3D CFD domain

7.2 Boundary condition

Boundary conditions are almost similar as applied before to 2D E-E VOF model. Inlet velocity profile is obtained from same formula for injection rate. For example, Inlet velocity profile is plotted in Figure 25, corresponding to case 2. Experimental results show the amount of liquid is present inside the pipe between the valves and the outlet of the nozzle before running the tests. Therefore, 50% liquid initiated in the pipe between the valves and the outlet of the nozzle as initial condition for preliminary results [Figure 25]

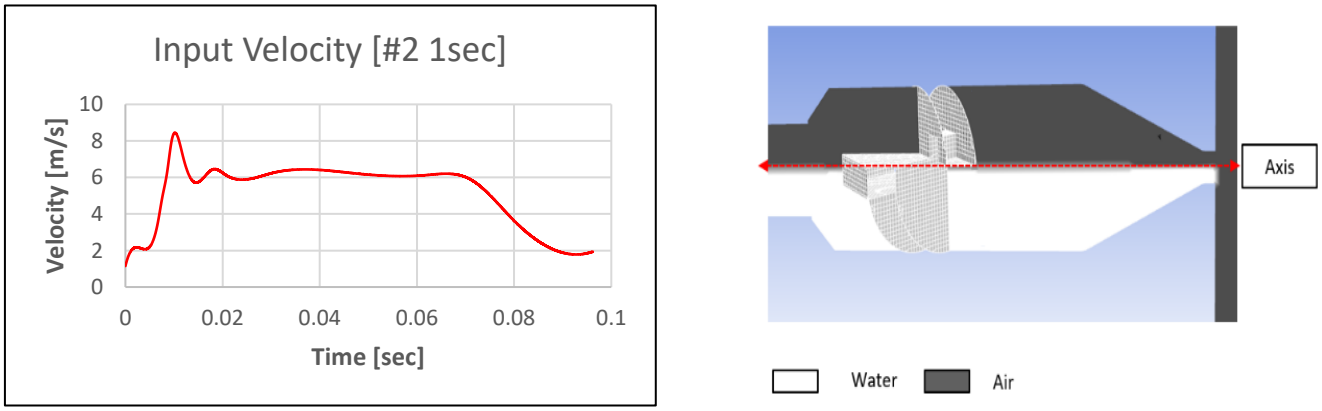

Figure 25 Inlet Boundary conditions

7.3 liquid level study

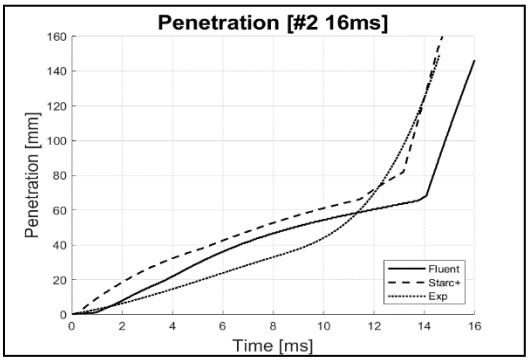

Figure 26 Preliminary penetration results

As can be seen in Figure 26, it shows non similar agreement between the experimental data and the simulation results in term of spray penetration is observed in the plot. It is observed that initial condition of liquid is present inside the pipe between the valves and the outlet of the nozzle is not good. For that reason, study of liquid present inside the pipe between the valves and the outlet of the nozzle carried out. As shown in figure 27, different amount of liquid is assumed as initial condition before simulation to calibrate the spray penetration with experimental data.

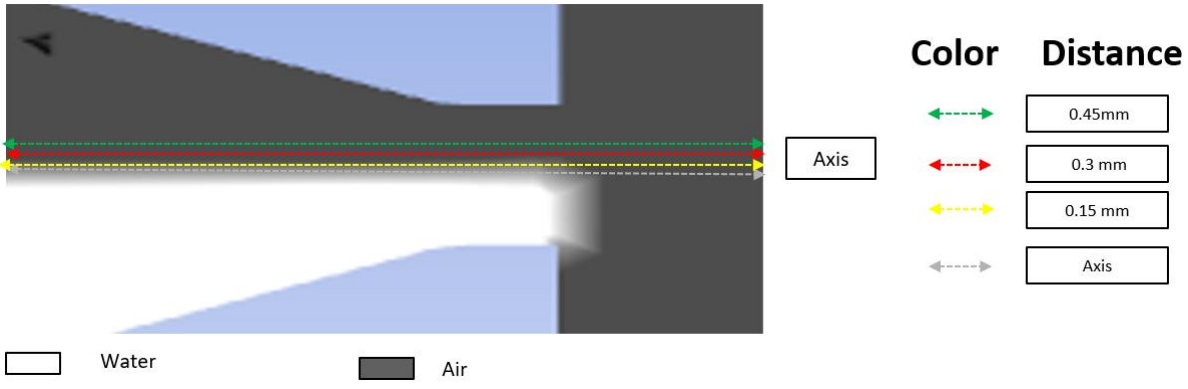

Figure 27 Different level of fluid in nozzle

Figure 28 shows the comparison of the liquid penetrations using different level of liquid present in nozzle before simulation versus time. In this figure plot, we could see the sizeable change in penetration with different level different level of liquid present in nozzle. It is observed that liquid present in the pipe with case 2 is be fitting for penetration curve. Therefore, for further all simulation we consider this condition as initial conditions.

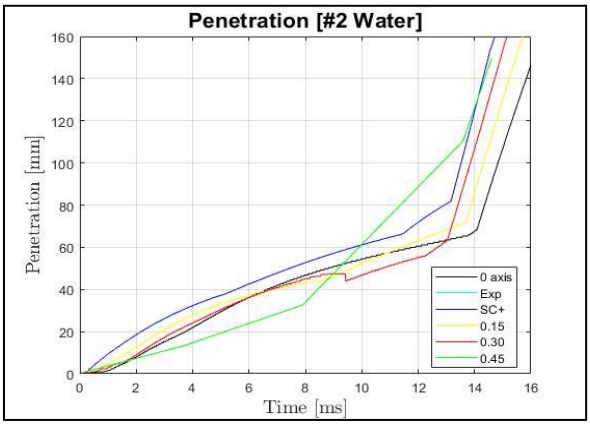

Figure 28 Penetration of different level of liqui

7.4 Results

Figure 29 shows the spray penetration results for the field of view 1 of four cases. The higher the injection pressure can lead to a faster spray penetrates the ambient. From figure it can observed that the shape of the curve changes from a parabolic trend to a straight line because in the first moments of the injection process the spray accelerates as it is injected.

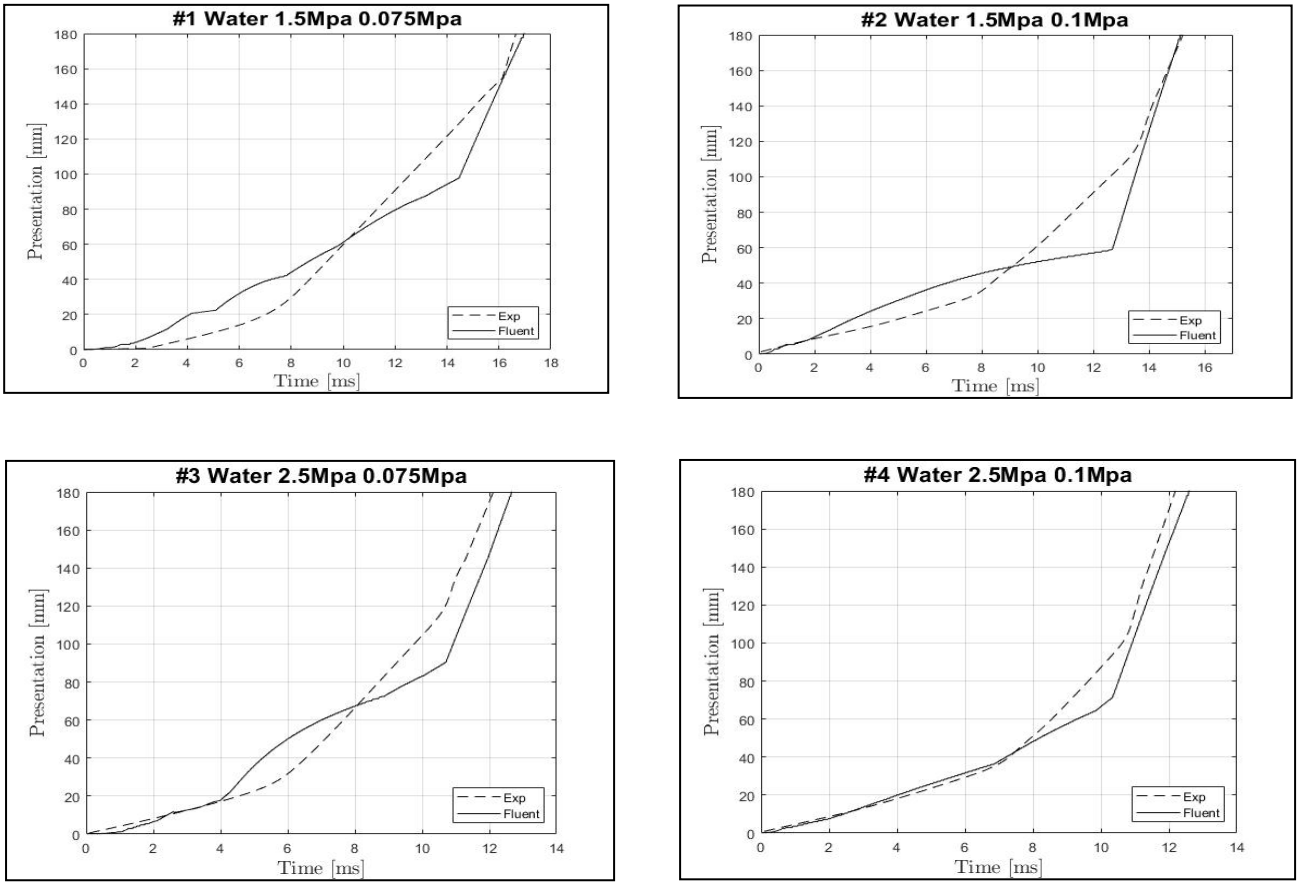

Figure 29 Spray penetration for different cases

Chapter 8

8 3D E- L model

8.1 Description

The purpose of this section is to make lagrangian model to analyze the full penetration curve. These simulations will be performed using the Discrete Phase Model (DPM) in the ANSYS Fluent program. DPM model in ANSYS Fluent uses the Euler-Lagrange approach. The Euler-Lagrange approach is much simpler to solve than the Euler-Euler approach [29]. The Eularian model is more accurate but more computationally expensive. This section ends with a comparison of penetration curve considering different break up models.

Figure 30 represent the simulation methodology which were performed during this project. Previously, Eulerian – Eulerian model simulated for both nozzle 1 and 2 to analyze the spray near nozzle part as knows as dense region. In real, the domain is very large. Therefore, DPM simulation which is Eulerian-Lagrangian approach is developed to analyze the spray of full domain.

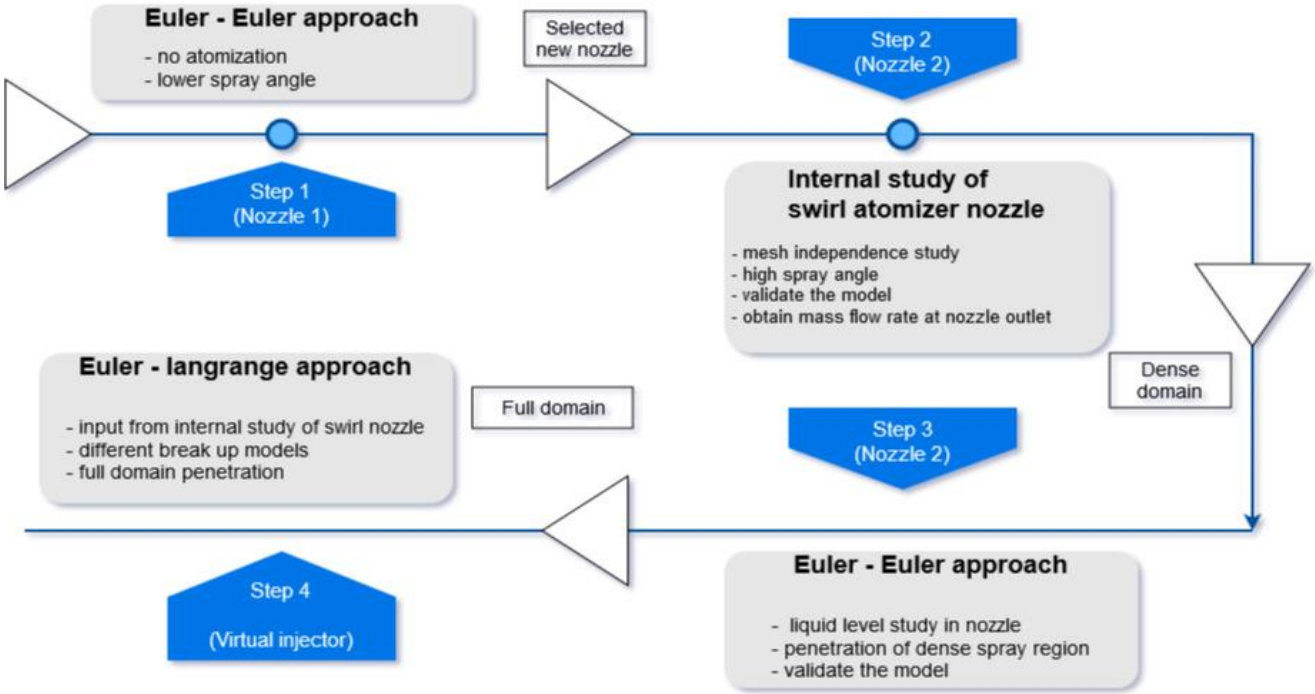

Figure 30 Workflow of simulation methodology

8.2 Geometry

In figure 31, cross section of 3D rectangular box 1200 x 300 x 300 mm is shown. Dimension of rectangular box is same scale as experimental box domain. For discrete phase model (DPM) simulation, domain which is shown in red box is neglected by creating new virtual injector.

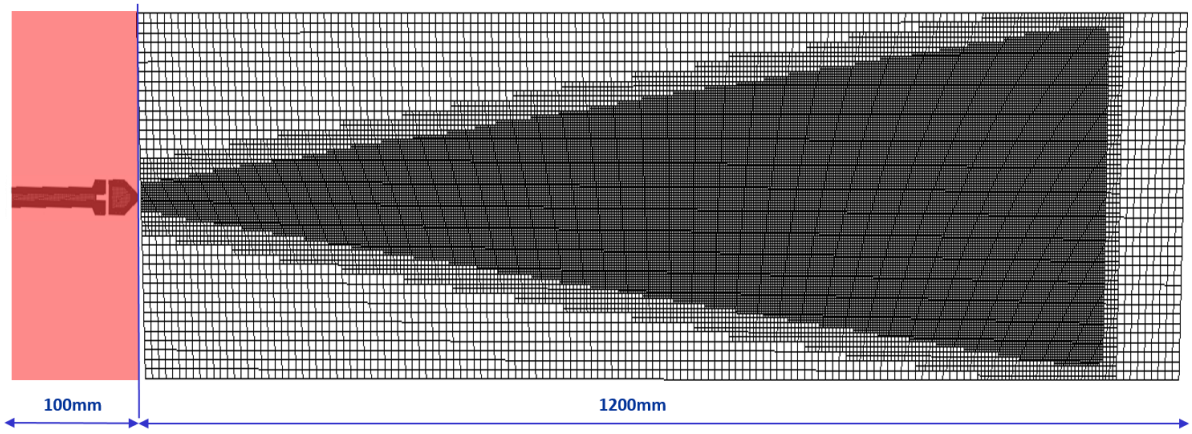

Figure 31 CFD domain for lagrangian simulation

8.3 Boundary conditions

The next step is to include the inlet boundary condition to the particle. the velocity profiles of water for four different cases which were directly obtained from study of internal characteristics of nozzle 2 (Figure 23). These profiles can be used as inlet boundary condition for virtual cone injector for full simulations.

8.4 Results

Figure 32 shows the entire spray penetration development for water along all the fields of views compare with experimental data. Dark highlighted data shown in experimental penetration curves represent the data capture from different field of view from camera. From its, full penetration line captured. The penetration near to the nozzle exit shown good curve trends compare to experimental data. It can be notice that higher injection pressure leads to faster spray penetration. the influence of the different break up models can be visualized. Also, it can be notice that trend of curve is almost similar with data. From figure 32, the penetration trend line for far to the nozzle where secondary atomization is happening not shown similar results as compare to experimental curve. Calibration of influence parameters in break up model are required to reduce such type of errors which can be future work of this project.

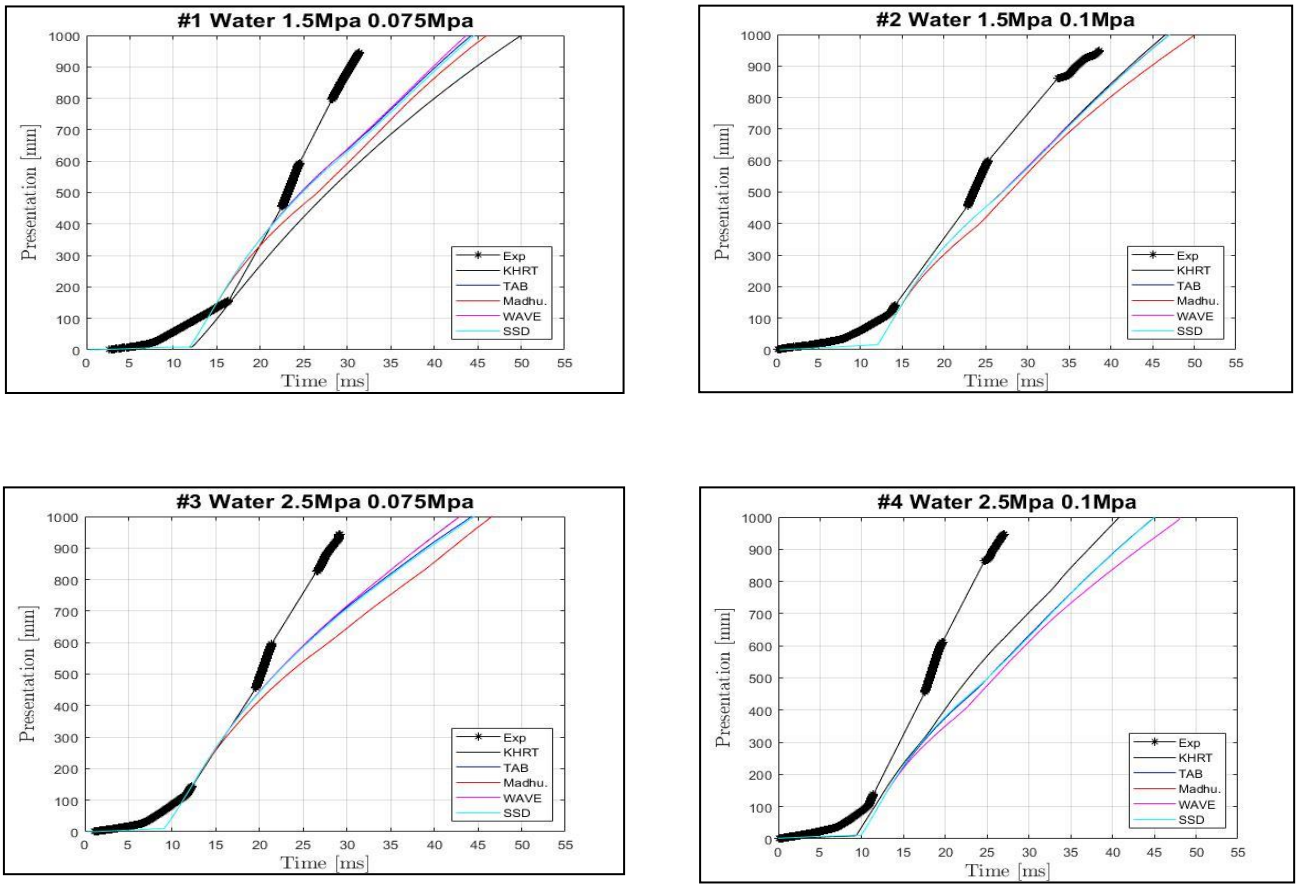

Figure 32 Comparison between different break up models

9 Conclusion

The main idea behind this thesis is to validate the Eulerian– Eulerian & Eulerian – Lagrangian model. All simulation model created and performed using CFD commercial software ANSYS Fluent. This conclusion is supported by following results:

- Eulerian–Eulerian VOF model was validated for Nozzle 1. It shows good agreement between experimental data and simulation data in terms of penetration for all cases of water and Novec1230.

- Results shows that water penetrates faster than Novce1230 into the volume and high injection pressure leads to faster penetration.

- Nozzle 1 sprays show low atomization with opening angles between 0.5◦ and 5◦. Therefore, nozzle 2 was selected in order to improve the spray atomization and to increase the cone spray angle as expected.

- Internal numerical study of nozzle 2 was carried out. Numerical investigation shows reasonably results compare to manufacture data sheet in internal nozzle flow development in terms of discharge coefficient, pressure difference of outlet and inlet of nozzle and spray angle.

- In addition, input boundary conditions obtained for Eulerian – Lagrangian model to run simulations without the nozzle geometry from internal numerical study of nozzle 2.

- 3D Eulerian–Eulerian VOF model was validated for nozzle 2. Preliminary results show that the air/fire agent mix present in the pipe between the valves.

- Liquid level studies show that the liquid present in the pipe between the valves can have large influence on penetration curve.

- 3D Eulerian – Lagrangian model simulation was run using the discrete phase model (DPM).

- 3D E-L simulations were performed considering different secondary breakup models. The wave and KHRT secondary breakup models were found to produce more close results for this case. It is recommended to be used for higher Reynolds numbers and higher Weber numbers.

References

[1] Elliott, D.G., Garrison, P.W., Klein, G.A., Moran, K.M., Zydowicz, M.P.: Flow of nitrogen-pressurized Halon 1301 in fire extinguishing systems. Tech. rep. (1984)

[2] Lefebvre, A.H., McDonell, V.G.: Atomization and sprays. CRC press (2017)

[3] Brennen C. “An oscillating-boundary-layer theory for ciliary propulsion”. Journal of Fluid Mechanics, Vol. 65, pp. 799–824, 10 1974.

[4] Reitz R. D. and Diwakar R. “Effect of Drop Breakup on Fuel Sprays”. SAE Technical Paper, no 860469, 1986.

[5] Reitz R. D. and Diwakar R. “Structure of High-Pressure Fuel Sprays”. SAE Technical Paper, no 870598, 1987.

[6] Lefebvre A.H. Atomization and sprays. Hemisphere Publishing Corporation, New York, 1989.

[7] Soteriou C., Andrews R. and Smith M. “Direct Injection Diesel Sprays and the Effect of Cavitation and Hydraulic Flip on Atomization”. SAE Technical Paper, no 950080, 1995.

[8] Morena J. Estudio de la influencia de las caracter´ısticas del flujo interno en toberas sobre el proceso de inyeccio´n Di´esel en campo pro´ximo. Doctoral Thesis, Departamento de Ma´quinas y Motores T´ermicos, Universidad Polit´ecnica de Valencia, Espana, 2011.

[9] Rayleigh L. “On The Instability Of Jets”. Proceedings of the London Mathematical Society, Vol. s1-10 no 1, pp. 4–13, 1878.

[10] Rayleigh L. “On the Capillary Phenomena of Jets”. Proceedings of the Royal Society of London, Vol. 29 no 196-199, pp. 71–97, 1879

[11] Haenlein A. “¨Uber den Zerfall eines Flu¨ssigkeitsstrahles”. Forschung auf dem Gebiet des Ingenieurwesens A, Vol. 2 no 4, pp. 139–149, 1931.

[12] Weber C. “Disintegration of Liquid Jets”. Z. Angew., Math. Mech., Vol. 11 no 2, pp. 136–154, 1931.

[13] Ohnesorge Wolfgang V. “Die Bildung von Tropfen an Du¨sen und die Aufl¨osung flu¨ssiger Strahlen”. ZAMM - Journal of Applied Mathematics and Mechanics / Zeitschrift fu¨r Angewandte Mathematik und Mechanik, Vol. 16 no 6, pp. 355–358, 1936.

[14] Reitz R. D. Atomization and other breakup regimes of a liquid jet. Doctoral Thesis, 08544, Princeton, New Jersey, United States of America: Princeton University, 1978.

[15] Reitz R. D. and Bracco F. V. “Mechanism of atomization of a liquid jet”. Physics of Fluids, Vol. 25 no 10, pp. 1730–1742, 1982.

[16] Pope, Stephen B. Turbulent Flows. 2001. doi: 10.1088/0957-0233/ 12/11/705.

[17] Reitz, R. D. and Bracco, F. V. “Mechanism of atomization of a liquid jet”. In: Physics of Fluids 25.10 (1982), pp. 1730–1742. doi: 10.1063/ 1.863650.

[19] ECN. ECN Webpage. https://aip.scitation.org/doi/10.1063/1.1756030

[20] Hirt, C.W., Nichols, B.D.: Volume of fluid (VOF) method for the dynamics of free boundaries. Journal of computational physics 39(1), 201–225 (1981)

[21] Jacqmin, D.: Calculation of two-phase Navier–Stokes flows using phase-field modelling. Journal of Computational Physics 155(1), 96–127 (1999)

[22] Baer, M., Nunziato, J.: A two-phase mixture theory for the deflagration to detonation transition (DDT) in reactive granular materials. International Journal of Multiphase Flow 12 (1986)

[23] Beard, K., Pruppacher, H.: A wind tunnel investigation of collection kernels for small water drops in air. Quarterly Journal of the Royal Meteorological Society 97(412), 242–248 (1971)

[24] Beji, T., Zadeh, S., Maragkos, G., B, M.: Influence of the particle injection rate, droplet size distribution and volume flux angular distribution on the results and computational time of water spray CFD simulations. Fire Safety Journal 91, 586– 595 (2017)

[25] Brown, P.P., Lawler, D.F.: Sphere drag and settling velocity revisited. Journal of Environmental Engineering 129(3), 222–231 (2003)

[26] Caupin, F., Herbert, E.: Cavitation in water: a review. Comptes Rendus Physique 7(9-10), 1000–1017 (2006)

[27] Floyd, J., McDermott, R.: Development and evaluation of two new droplet evaporation schemes for fire dynamics simulations. Fire Safety Journal 91, 643–652 (2017)

[28] Fluent, A.: 18.0 ANSYS Fluent theory guide 18.0. Ansys Inc (2017)

[29] Fraysse, F., Redondo, C., Rubio, G., Valero, E.: Upwind methods for the Baer– Nunziato equations and higher-order reconstruction using artificial viscosity. Journal of Computational Physics 326, 805–827 (2016)

[30] Schwarzkopf, J.D., Sommerfeld, M., Crowe, C.T., Tsuji, Y.: Multiphase flows with droplets and particles. CRC press (2011)

[31] McGrattan, K., Hostikka, S., McDermott, R., Floyd, J., Weinschenk, C., Overholt, K.: Fire dynamics simulator technical reference guide volume 1: mathematical model. NIST special publication 1018(1), 175 (2013)

[32] Mahmud, H.: Simulation of the suppression of fires using water mists. Ph.D. thesis, Victoria University (2016)

[33] Garcia-Oliver, J.M., Pastor, J.M., Pandal, A., Trask, N., Baldwin, E., Schmidt, D.P.: Diesel spray CFD simulations based on the Σ-Y Eulerian atomization model. Atomization and Sprays 23(1) (2013)

[35] Vallet, A., Borghi, R.: An Eulerian model of atomization of a liquid jet. Comptes Rendus de l'Academie des Sciences Series IIB Mechanics Physics Astronomy 327(10), 1015–1020 (1999)

[36] Henrik Rusche. Computational fluid dynamics of dispersed two-phase flows at high phase fractions. PhD thesis, Imperial College London (University of London), 2003.

[37] Fluent, A.: 18.0 ANSYS Fluent theory guide 18.0. Ansys Inc (2017)

[38] Morsi, S., Alexander, A.: An investigation of particle trajectories in two-phase flow systems. Journal of Fluid mechanics 55(2), 193–208 (1972)

[39] P. Spalart and S. Allmaras. "A one-equation turbulence model for aerodynamic flows". Technical Report AIAA-92-0439. American Institute of Aeronautics and Astronautics. 1992.

[40] B. E. Launder and D. B.Spalding. "The Numerical Computation of Turbulent Flows". Computer Methods in Applied Mechanics and Engineering. 3. 269–289. 1974.

[41] V. Yakhot and S. A. Orszag. "Renormalization Group Analysis of Turbulence I Basic Theory". Journal of Scientific Computing. 1(1). 1–51. 1986.

[42] T.-H. Shih, W. W. Liou, A. Shabbir, Z. Yang, and J. Zhu. "A New - Eddy-Viscosity Model for High Reynolds Number Turbulent Flows - Model Development and Validation". Computers Fluids. 24(3). 227–238. 1995.

[43] D. C. Wilcox. Turbulence Modeling for CFD. DCW Industries, Inc. La Canada, California. 1998.

[44] F.R.Menter. "Two-Equation Eddy-Viscosity Turbulence Models for Engineering Applications". AIAA Journal. 32(8). 1598–1605. August 1994

[45] Reitz, R. D. "Atomization and other breakup regimes of a liquid jet". PhD thesis. 08544, Princeton, New Jersey, United States of America: Princeton University, 1978

[46] Som, S. and S. K. Aggarwal. "Effects of primary breakup modeling on spray and combustion characteristics of compression ignition engines". Combustion and Flame, vol. 157.6 (2010), pp. 1179–1193

[47] O'Rourke, P. J. and A. A. Amsden. "The Tab Method for Numerical Calculation of Spray Droplet Breakup". SAE Technical Paper 872089 (1987).

[48] Senecal, P. K. et al. "Modeling high-speed viscous liquid sheet atomization" International Journal of Multiphase Flow, vol. 25.6-7 (1999)

[49] Dombrowski, N. and W. R. Johns. "The aerodynamic instability and disintegration of viscous liquid sheets". Chemical Engineering Science, vol. 18.3 (1963), pp. 203–214

[50] Reitz,R.D.and R.Diwakar." Effect of Drop Breakup on Fuel Sprays". SAE Technical Paper 860469 (1986)

[51] Pilch, M. M. and C. A. Erdman. “Use of breakup time data and velocity history data to predict the maximum size of stable fragments for acceleration-induced breakup of a liquid drop”. International Journal of Multiphase Flow, vol. 13.6 (1987)

[52] Hsiang, L.-P. and G. M. Faeth. “Near-limit drop deformation and secondary breakup”. International Journal of Multiphase Flow, vol. 18.5 (1992)

[53] Chu, C. C. and M. L. Corradini. “One-dimensional transient fluid model for fuel/coolant interaction analysis”. Nuclear Science and Engineering, vol. 101.1 (1989)

[54] Patterson, M. A. and R. D. Reitz. “Modeling the Effects of Fuel Spray Characteristics on Diesel Engine Combustion and Emission”. SAE Technical Paper 980131 (1998)

Annex 1 Nozzle dimension

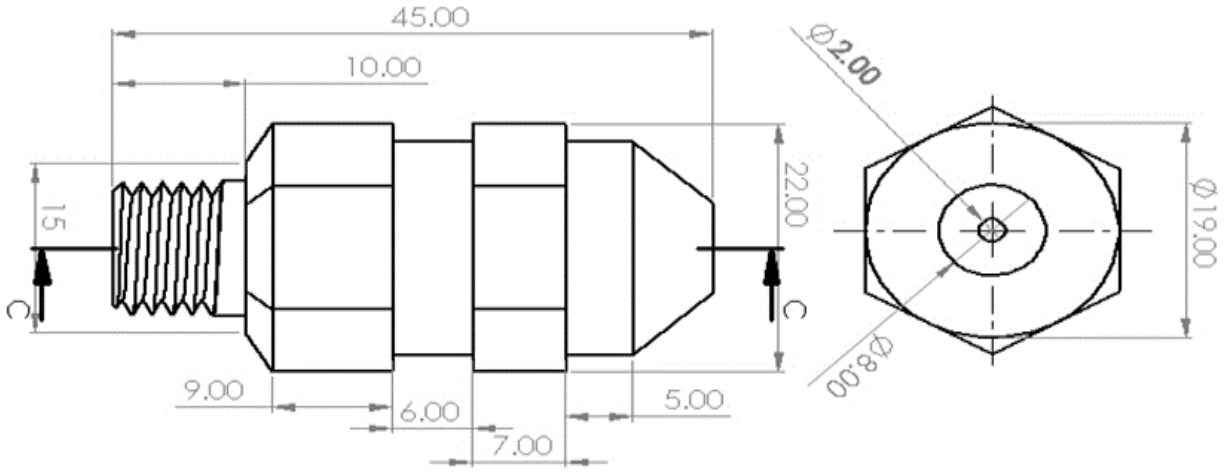

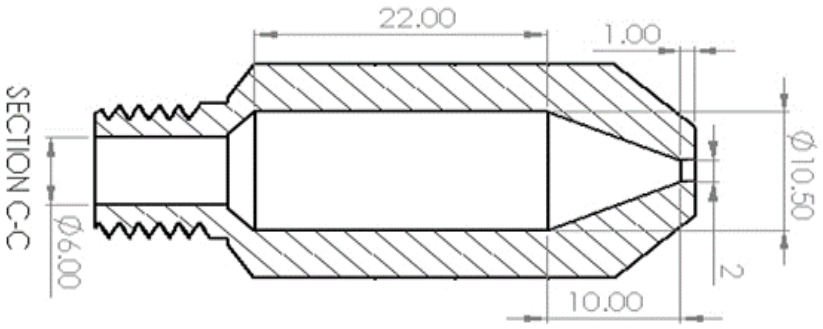

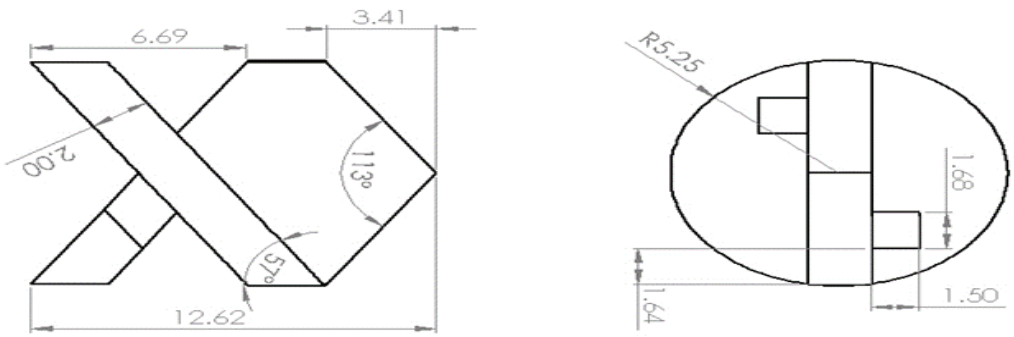

Annex 2 Test matrix

Case	Fluid	Injection Pressure	Ambient gas Pressure	Temperature
[-]	[-]	[Mpa]	[Mpa]	[K]
1	Water	1.5	0.1	298
2			0.075	
3		2.5	0.1	
4			0.075	
5	Novec	1.5	0.1	258
6				278
7				298
8			0.075	278
9				298
10		2.5	0.1	258
11				278
12				298
13			0.075	278
14				298

Table of different test parameters performed at CMT testing facilities